# **UC Berkeley**

# **UC Berkeley Previously Published Works**

### **Title**

Responses of Marginal and Intrinsic Water-Use Efficiency to Changing Aridity Using FLUXNET Observations

#### **Permalink**

https://escholarship.org/uc/item/54m1b3t8

### **Journal**

Journal of Geophysical Research: Biogeosciences, 129(6)

#### **ISSN**

2169-8953

### **Authors**

Yi, Koong Novick, Kimberly A Zhang, Quan et al.

### **Publication Date**

2024-06-01

#### DOI

10.1029/2023jg007875

### **Copyright Information**

This work is made available under the terms of a Creative Commons Attribution License, available at <a href="https://creativecommons.org/licenses/by/4.0/">https://creativecommons.org/licenses/by/4.0/</a>

Peer reviewed

# 1 Responses of marginal and intrinsic water-use efficiency to changing aridity

# 2 using FLUXNET observations

3

- 4 Koong Yi<sup>1</sup>, Kimberly A. Novick<sup>2</sup>, Quan Zhang<sup>3</sup>, Lixin Wang<sup>4</sup>, Taehee Hwang<sup>5</sup>, Xi Yang<sup>6</sup>,
- 5 Kanishka Mallick<sup>7,8</sup>, Martin Béland<sup>7,9</sup>, Gabriel B. Senay<sup>10</sup>, Dennis Baldocchi<sup>7</sup>

6

- <sup>1</sup>Earth and Environmental Sciences Area, Lawrence Berkeley National Laboratory, CA, U.S.A.
- <sup>2</sup>O'Neill School of Public and Environmental Affairs, Indiana University Bloomington,
- 9 Bloomington, IN, U.S.A.
- <sup>3</sup>State Key Laboratory of Water Resources and Hydropower Engineering Science, Wuhan
- 11 University, Wuhan, China.
- <sup>4</sup>Department of Earth Sciences, Indiana University-Purdue University Indianapolis (IUPUI),
- 13 Indianapolis, IN, U.S.A.
- <sup>5</sup>Department of Geography, Indiana University Bloomington, Bloomington, IN, U.S.A.
- <sup>6</sup>Department of Environmental Sciences, University of Virginia, Charlottesville, VA, U.S.A.
- <sup>7</sup>Department of Environmental Science, Policy, and Management, University of California,
- 17 Berkeley, CA, U.S.A.
- <sup>8</sup>Department of Environment Research and Innovation, Luxembourg Institute of Science and
- 19 Technology, Belvaux, Luxembourg
- <sup>9</sup>Department of Geomatics Sciences, Laval University, Quebec City, Quebec, Canada
- <sup>10</sup>U.S. Geological Survey Earth Resources Observation and Science Center, North Central
- 22 Climate Adaptation Science Center, Fort Collins, CO, U.S.A.

- 24 Corresponding Author:
- 25 Koong Yi
- 26 Email: koongyi@gmail.com
- 27 Phone: +1-812-650-2930

28

29

30

31

32

33

34

35

36

37

38

39

40

41

42

43

44

45

46

#### Abstract

According to classic stomatal optimization theory, plant stomata are regulated to maximize carbon assimilation for a given water loss. A key component of stomatal optimization models is marginal water-use efficiency (mWUE), the ratio of the change of transpiration to the change in carbon assimilation. Although the mWUE is often assumed to be constant, variability of mWUE under changing hydrologic conditions has been reported. However, there has yet to be a consensus on the patterns of mWUE variabilities and their relations with atmospheric aridity. We investigate the dynamics of mWUE in response to vapor pressure deficit (VPD) and aridity index using carbon and water fluxes from 115 eddy covariance towers available from the global database FLUXNET. We demonstrate a non-linear mWUE-VPD relationship at a sub-daily scale in general; mWUE varies substantially at both low and high VPD levels. However, mWUE remains relatively constant within the mid-range of VPD. Despite the highly non-linear relationship between mWUE and VPD, the relationship can be informed by the strong linear relationship between ecosystem-level inherent water-use efficiency (IWUE) and mWUE using the slope,  $m^*$ . We further identify site-specific  $m^*$  and its variability with changing site-level aridity across six vegetation types. We suggest accurately representing the relationship between IWUE and VPD using Michaelis-Menten or quadratic functions to ensure precise estimation of mWUE variability for individual sites.

	$\neg$
/	- /

## Plain Language Summary

Plants use diverse strategies for water utilization during growth. Marginal water-use efficiency (mWUE) quantifies how effectively plants gain carbon relative to the water they lose through their leaves. A scientific debate exists regarding how mWUE responds to dry conditions. To investigate this, we analyze data from various vegetation types worldwide, observing changes in mWUE under dry conditions. Contrary to common assumptions, mWUE is not a constant; it varies substantially based on moisture levels. Additionally, we show that a simpler measure called inherent water-use efficiency (IWUE) can help explain this complicated relationship, which is useful for predicting plant growth under different moisture conditions.

# Keywords

- Climate change, drought, eddy covariance, stomatal optimization theory, vapor pressure deficit,
- 60 water-use efficiency

# Running title

Response of mWUE and IWUE to changing aridity

### 1. Introduction

Terrestrial plants mitigate global warming by sequestering atmospheric carbon dioxide (CO<sub>2</sub>) through photosynthesis (Beer et al., 2010). However, photosynthesis is inherently linked with plant water loss via transpiration, as CO<sub>2</sub> and water vapor share the same stomatal pathway. Plants risk hydraulic damage during droughts if they maintain high stomatal conductance as soil water availability decreases and atmospheric demand increases, resulting in low leaf water potential and xylem cavitation. Therefore, plants must balance stomatal function to optimize carbon uptake while minimizing transpirational water loss and hydraulic stress (Cowan & Farquhar, 1977; Katul et al., 2010; Sperry et al., 2017; Wang et al., 2020). To predict plant ecophysiological responses to projected changes in atmospheric CO<sub>2</sub> concentration, elevated atmospheric water demand, and more severe and frequent drought events, we need a mechanistic understanding of how different ecosystems regulate the trade-off between photosynthetic carbon assimilation and transpirational water loss.

Although carbon uptake is usually represented through mechanistic models of photosynthesis (e.g., the Michaelis-Menten equation (Marshall & Biscoe, 1980; Michaelis & Menten, 1913; Thornley, 1976); the Farquhar model (Von Caemmerer, 2000; Farquhar et al., 1980a)), water use (i.e., transpiration) is often described based on empirical relationships that prescribe how stomatal conductance responds to environmental drivers and carbon uptakes. For example, the Ball-Berry model (Ball et al., 1987) is one of the most widely used empirical stomatal conductance models (Anderegg et al., 2017; Buckley, 2017; Katul et al., 2010), and has been readily incorporated into many climate models (Bonan et al., 2014). It takes the form:

$$g_s = g_0 + g_1 \frac{A}{c_a} \text{RH} \qquad (1)$$

where  $g_s$  is stomatal conductance (mol m<sup>-2</sup> s<sup>-1</sup>), A is carbon assimilation rate ( $\mu$ mol m<sup>-2</sup> s<sup>-1</sup>),  $c_a$  is atmospheric CO<sub>2</sub> concentration (ppm), RH is relative humidity at the leaf surface, and  $g_0$  and  $g_1$  are empirically fitted parameters. To simulate the non-linear variation in  $g_s$  with changing humidity, Leuning (1995) modified the Ball-Berry model by replacing relative humidity with a vapor pressure deficit (VPD) response function as follows:

$$g_s = g_0 + g_1 \cdot \frac{A}{(c_a - \Gamma^*) \left(1 + \frac{\text{VPD}}{\text{VPD}_0}\right)}$$
 (2)

where  $\Gamma^*$  is CO<sub>2</sub> compensation point for photosynthesis (ppm) and VPD<sub>0</sub> is the empirically determined coefficient, representing the slope of the relationship between  $g_s$  and VPD. These empirical models are relatively simple, easy to use, and work well for well-watered conditions (Bonan et al., 2014). However, they have an incomplete grounding in physiological theory, leading to uncertainty when they are extrapolated to predict plant function under unprecedented climate conditions (Franks et al., 2018; Knauer et al., 2015, 2018; Medlyn et al., 2012; Sabot et al., 2022).

An alternative way to enable the theoretical interpretation of leaf-level stomatal conductance models is to adopt the principle of stomatal optimization theory (Anderegg et al., 2018; Bonan et al., 2014; Katul et al., 2009; Katul et al., 2010; Medlyn et al., 2012; Novick et al., 2016b; Sperry et al., 2017; Wolf et al., 2016). Stomatal optimization theory was originally based on a hypothesis that stomata are regulated to maximize carbon assimilation (A) for a given water loss (transpiration, E). A key parameter in this class of models is the so-called "marginal wateruse efficiency (mWUE)," here defined as the ratio of a change in E to a change in A ( $\partial E/\partial A$ ) following Cowan and Farquhar (1977), although it is sometimes defined as the inverse form ( $\partial A/\partial E$ ) (Katul et al., 2010; Manzoni et al., 2011). The optimality models often maintain the mWUE constant over arbitrary time steps (e.g., daily), assuming abundant water at the canopy

(Buckley, 2017; Cowan & Farquhar, 1977; Makela et al., 1996). However, this may not hold true at sub-daily timescales, where high atmospheric demand (i.e., VPD) during midday can decrease water potential at the canopy level even when soil moisture is abundant (Anderegg et al., 2017; Grossiord et al., 2020).

109

110

111

112

113

114

115

116

117

118

119

120

121

122

123

124

125

126

127

128

129

130

131

Understanding how mWUE changes under hydrologic stress is necessary for the optimization models in a prognostic sense, yet no consensus on the magnitude or even direction of these changes exists. For instance, Manzoni et al. (2011) and Zhou et al. (2013, 2014) performed meta-analyses of leaf gas exchange measurements from previous studies that spanned wide ranges of species and moisture conditions. A major difference in their approaches was the proxy for plant water status; Manzoni et al. (2011) used mid-day leaf water potential, whereas Zhou et al. (2013, 2014) used pre-dawn leaf water potential as a proxy for soil moisture availability. Similarly, Lin et al. (2015) compiled a global database of leaf gas exchange measurements spanning diverse plant functional types and estimated a slope parameter  $(g_1)$ (Medlyn et al., 2012), which is analogous to the slope parameter from empirical models (Eqs. 1 & 2) and proportional to  $\sqrt{\partial E/\partial A}$  (Medlyn et al., 2012). They further evaluated the relationship between  $g_1$  and a moisture index, defined as the ratio of mean annual precipitation to the equilibrium evapotranspiration. Mäkelä et al. (1996) and Lu et al. (2016) took a theoretical approach to examine short- and long-term optimal stomatal behavior, respectively, in response to the soil moisture availability assuming that plants are adapted to the stochastic rainfall patterns of their environments. More recently, alternative stomatal optimization perspectives have been proposed, which presume stomata function to maximize carbon uptake while minimizing water costs, including those linked to hydraulic damage during droughts (Anderegg et al., 2018; Sperry et al., 2017; Wolf et al., 2016). Although promising, in contrast to the Medlyn et al. (2012)

model, these newer formulations have yet to be integrated into land surface model schemes (but refer to Kennedy et al., 2019, for a study implementing plant hydraulics in the Community Land Model). Although theoretical expectation and many studies indicate decreasing mWUE as water stress drives reductions to  $g_s$ , there is some evidence of increasing mWUE under water stress (Farquhar et al., 1980b; Grieu et al., 1988; Zhou et al., 2013), although reasons for this needed to be clarified.

132

133

134

135

136

137

138

139

140

141

142

143

144

145

146

147

148

149

150

151

152

153

154

It is also important to note that canopy water status and water potential are not determined solely by the availability of water supply but by the balance between water supply and demand, with VPD as a major force exerted on the canopy by the atmosphere (Manzoni et al., 2011, 2013; Novick et al., 2019). Thus, it is reasonable to expect that mWUE needs to be adjusted with changing atmospheric water demand unless other factors limit the plant response (e.g., compromised hydraulic conductivity under water stress, limited soil moisture availability to plants) (Brodribb et al., 2005; Medlyn et al., 2012). Different plants or ecosystems may adjust differently, resulting in divergent responses of mWUE to changing VPD. Understanding the relationship between mWUE and VPD is important given that VPD is expected to keep increasing in the future, which will exert further water stress on plants (Ficklin & Novick, 2017; Grossiord et al., 2020; Novick et al., 2016a; Zhang et al., 2019). Furthermore, while soil moisture is a stochastic variable due to its dependency on intermittent rainfall, VPD is smoother in time and easier to monitor through various meteorological or gas exchange measurement techniques. Although VPD and soil moisture limit plants' carbon uptake and water use independently (Yi et al., 2019), VPD can be used as a proxy of water stress at a sub-daily scale where VPD plays a primary role in regulating stomatal regulation unless severe soil moisture deficiency, as indicated by the models with sub-daily timesteps (e.g., Ball-Berry model and its

variations), and in turn influencing the balance between carbon uptake and water loss (i.e., water-use efficiency) at a sub-daily scale (Baldocchi et al., 2022; Grossiord et al., 2020; Novick et al., 2016a). Therefore, examining the association between mWUE and VPD would add insight into the predictability of soil moisture alone.

The objectives of this study are (1) to investigate the variation of mWUE at an hourly timescale in response to changing VPD and (2) to explore approaches for estimating mWUE explicitly from the modeled relationship between intrinsic water-use efficiency (iWUE, carbon assimilation per unit stomatal conductance, representing water-use efficiency at leaf level) and VPD. The Ball-Berry model (Eq. 1) reveals that the parameter  $g_1$ , which is proportional to  $\sqrt{\partial E/\partial A}$  (Medlyn et al., 2012), is related to  $A/g_s$  (= iWUE at leaf level). The iWUE can be more straightforwardly estimated from field measurements across various spatiotemporal scales, including leaf gas exchange (daily to weekly at the leaf level), dendrochronology (seasonal/annual at the tree level), and eddy covariance (hourly at the stand level) (more discussion on iWUE at different scales is available from Beer et al., 2009 and Yi et al., 2019). Notably, the inference of iWUE from tree-ring analyses provides an avenue for understanding historical variations in iWUE and, potentially, mWUE. While iWUE has a mathematically simpler form and thus facilitates modeling its response to water stress, the complex mathematical expression of mWUE poses challenges in generalizing its variability at a sub-daily timescale. By elucidating the correlation between iWUE and mWUE, we can gain insights into the response of mWUE to water stress. Additionally, through site comparisons, we further explore whether there is an emerging pattern in the correlation between iWUE and mWUE across different vegetation types and aridity levels.

155

156

157

158

159

160

161

162

163

164

165

166

167

168

169

170

171

172

173

174

175

Table 1. A glossary of terms related to water-use efficiency.

Term or symbol	Definition
$\overline{A}$	Carbon assimilation rate
AI	Aridity index: the ratio of annual precipitation to annual potential evapotranspiration
$C_{\mathrm{a}}$	Atmospheric CO <sub>2</sub> concentration
E	Transpiration rate
ET	Evapotranspiration rate
$g_0$	Intercept parameter in Ball-Berry model (represents minimum leaf conductance)
$g_1$	Slope parameter in Ball-Berry model (represents marginal water-use efficiency, mWUE)
$g_{\rm s}$	Stomatal conductance
$G_{\mathrm{s}}$	Surface conductance
GPP	Gross primary productivity
iWUE	Intrinsic water-use efficiency; leaf-level water-use efficiency (= $A / g_s$ )
IWUE	Inherent water-use efficiency; a proxy of intrinsic water-use efficiency at the ecosystem level (= GPP / ET $\times$ VPD / $P_a$ , Beer et al., 2009)
m*	The slope of the linear relationship between IWUE <sup>-1</sup> and mWUE
mWUE	Marginal water-use efficiency, the ratio of a change in $E$ to a change in $A$ (= $\partial E/\partial A$ )
$P_{\mathrm{a}}$	Atmospheric pressure
VPD	Vapor pressure deficit

## 2. Materials and Methods

### 2.1. FLUXNET data

We obtained half-hourly measurements of carbon and energy fluxes, along with ancillary environmental data, from 115 flux towers across FLUXNET sites. These data were collected using the FLUXNET 2015 Tier 1 database (Table S1) (Pastorello et al., 2020). Eddy covariance records, which have the benefit of providing continuous meteorological and gas exchange data at

the high temporal resolution, are very well suited for investigating the relationship between gas exchange dynamics, mWUE, and VPD at the ecosystem scale.

186

187

188

189

190

191

192

193

194

195

196

197

198

199

200

201

202

203

204

205

206

207

208

We selected the study sites from six vegetation types (grassland, cropland, shrubland, savanna, broadleaf forest, and needleleaf forest, based on the International Geosphere-Biosphere Programme (IGBP) land cover classification system; Loveland & Belward, 1997) based on the data availability for the variables required for the analysis. For reliable and clear mWUE analysis, we only included the sites that had at least three years of data and a strong iWUE-VPD correlation. Specifically, we selected the sites that had a coefficient of determination  $(R^2) > 0.8$ with any of the three model fits—linear, quadratic, or Michaelis-Menten, which was the case for more than 70% of the sites over three years of data (refer to section 2.4 for more information about the model fits). In addition, we only used the data where net ecosystem exchange (NEE), latent heat flux (LE), and sensible heat flux (H) were either original measurements (quality control flag = 0) or gap-filled data of good quality (quality control flag = 1) to ensure data quality and make the most of the data. We only used daytime data when net radiation was greater than 0 W m<sup>-2</sup> without precipitation. While we acknowledge the potential benefits of excluding more days after rainfall (e.g., Lin et al., 2015), we believe that omitting only the precipitation days is sufficient for our analysis. This is because iWUE had low variability under humid conditions, as evidenced by the low standard deviations of IWUE under low VPD levels in Figure 2. Additionally, we implemented a procedure to remove outliers in soil water content and relative humidity as described in the following paragraph, which would help mitigate the impact of periods after rainy days on our analysis.

We limited our analysis to the growing season, where daily GPP was larger than 10% of the  $95^{th}$  percentiles of daily GPP for each site with  $> 5^{\circ}$ C air temperature. We used the GPP

partitioned based on the standard daytime method (variable name: GPP\_DT\_VUT\_REF, Lasslop et al., 2010). Additional filtering criteria were applied for some key variables: atmospheric CO<sub>2</sub> concentration between 350 ppm and 420 ppm, friction velocity ( $u^*$ ) greater than 0.1 m s<sup>-1</sup>, and canopy conductance calculated by Penman-Monteith equation (Monteith, 1965) greater than 0.05 mol m<sup>-2</sup> s<sup>-1</sup>. Lastly, we removed outliers of the environmental drivers and biological variables (i.e., air temperature, relative humidity, atmospheric CO<sub>2</sub> concentration, latent heat flux, wind speed, VPD, atmospheric pressure, friction velocity, net radiation, soil water content, canopy conductance, iWUE, and mWUE) by excluding data that were below the 5<sup>th</sup> or above the 95<sup>th</sup> percentiles of each variable. Note that the purpose of data filtering was to remove exceptionally low or high values of the variables, which we consider outliers. Our goal was to ensure that the results, especially the variability of mWUE, were not unduly influenced by these outliers. We carefully examined the histograms for the variables for each site to minimize data reduction while retaining useful information.

### 2.2. Two different approaches describing mWUE

We used two different approaches for describing the mWUE: two optimization-theory-driven mWUE, the solution of " $\partial E/\partial A$ " suggested by Katul et al. (2010) and the " $g_1$ " parameter proposed by Medlyn et al. (2012). The difference between the optimization-theory-driven mWUE is based on their interpretation of stomatal optimization. Katul et al. (2010) assumed that stomata are optimizing for photosynthesis limited by Rubisco activity (i.e., carbon-limited), and plant stomatal optimality is subject to change (i.e., mWUE is not constant). On the other hand, Medlyn et al. (2012) assumed that stomata are optimized for photosynthesis limited by Ribulose-1,5-bisphosphate (RuBP) regeneration (i.e., light-limited). In either case, the optimization

objective should result in constant mWUE values at short timescales—Katul et al. (2010) 232 suggested approximately 10 minutes, whereas Medlyn et al. (2012) suggested daily or longer— 233 although it may change at longer timescales as hydrologic conditions evolve.

Following Katul et al. (2010), the  $\partial E/\partial A$  emerges from an optimality condition determined with a linearized variant of the Farquhar et al. (1980b) photosynthesis model, defined as:

$$\frac{\partial E}{\partial A} = 1.6 \text{ VPD } c_a \left(\frac{A}{g_s}\right)^{-2} = \frac{1.6 \text{ VPD } c_a}{\text{iWUE}^2}$$
 (3)

234

235

236

237

248

251

where iWUE is defined as a ratio of A to  $g_s$  at the leaf-scale (Beer et al., 2009). 239

The other perspective on optimality proposed by Medlyn et al. (2012) takes an analogous 240 form to an empirical model proposed by Leuning (1995) (Eq. 2): 241

$$g_s \approx g_0 + 1.6 \left( 1 + \frac{g_1}{\sqrt{\text{VPD}}} \right) \frac{A}{c_a}$$
 (4)

This approach indicates that the parameter  $g_1$  represents a slope between  $g_s$  and  $A/c_a\sqrt{\text{VPD}}$  and 243 is proportional to  $\sqrt{\partial E/\partial A}$  (Lin et al., 2015; Medlyn et al., 2012). Therefore, to facilitate 244 comparison between the two approaches, we compare  $\partial E/\partial A$  with squared  $g_1$  (i.e.,  $g_1^2$ ) 245 throughout the results. Eq. 4 was rearranged with an assumption that  $g_0$ , which represents 246 cuticular conductance to water vapor, is negligible (but refer to Manzoni et al. (2011) and 247

$$g_1 = \left(\frac{g_s c_a}{1.6 A} - 1\right) \sqrt{\text{VPD}} = \left(\frac{c_a}{1.6 \text{ iWUE}} - 1\right) \sqrt{\text{VPD}}$$
 (5)

Consequently, two different mWUE parameters,  $\partial E/\partial A$  (mol H<sub>2</sub>O · kPa · mol<sup>-1</sup> of dry air) and  $g_1$ 250

Lanning et al. (2020) for discussion of the role of cuticle conductance under drier conditions):

(mol  $H_2O \cdot kPa^{0.5} \cdot mol^{-1}$  of dry air), were expressed as functions of iWUE,  $c_a$ , and VPD.

Assuming  $c_a$  is relatively stable over a short period, we focus on how iWUE (as a biological 252 factor) and VPD (as an indicator of water stress governing plant response at a short temporal 253 scale, e.g., sub-daily) affect both mWUE parameters (more details discussed in section 2.5). We 254

applied an approximation of iWUE at the ecosystem level, inherent WUE (IWUE), defined by Beer et al. (2009). IWUE ( $\mu$ mol C mol<sup>-1</sup> H<sub>2</sub>O) was particularly suitable for our study because IWUE can be calculated from the measurements of carbon and water fluxes by eddy covariance technique and ancillary meteorological data, i.e., gross primary productivity (GPP;  $\mu$ mol m<sup>-2</sup> s<sup>-1</sup>) from net ecosystem exchange representing canopy-level carbon assimilation, evapotranspiration rate (ET, mol m<sup>-2</sup> s<sup>-1</sup>) from latent heat flux, VPD under the assumption of equal temperatures of leaves and atmosphere, and atmospheric pressure ( $P_a$ , kPa):

$$IWUE = \frac{GPP \cdot VPD}{ET \cdot P_a}$$
 (6)

Several important assumptions for the definition of IWUE include (1) small and invariant soil evaporation (E) compared to plant transpiration (T) over the course of the day (hence  $\Delta ET \sim \Delta T$ ) especially during days without rainfall (conditions we used for our analysis), (2) thermal equilibrium between leaf and air, which influences VPD, and (3) disregarding of aerodynamic resistance through the boundary layer that can change depending on the vegetation structure (refer to Beer et al. (2009) for more discussion about IWUE as a proxy of ecosystem-level iWUE). We confirmed the robustness of IWUE as a proxy of iWUE at the ecosystem level by comparing it with a few other definitions of iWUE (the comparison results are available in the Supporting Information; Figs. S1 & S2). Note that IWUE and mWUE were computed using half-hourly FLUXNET data; hence, their variabilities discussed here represent plant physiological response at a sub-hourly scale.

### 2.3. Sensitivity of mWUE parameters to moisture condition

Variations of mWUE parameters in response to moisture conditions (i.e., atmospheric water demand and site-level aridity) were evaluated at the individual site level and across sites. For the individual sites, mWUE parameters were partitioned into discrete bins spanning a range of VPD. To avoid biases from unevenly distributed data points across the range of VPD (i.e., sample sizes at low and high VPD are smaller than those for the intermediate level of VPD), data binning was performed in a way that the sample sizes were evenly distributed into 30 bins across the range of VPD at each site. Then, mWUE-VPD relationships were produced based on the mean mWUE values generated for the different VPD bins.

To compare across the sites, the relationships between site-specific mWUE and aridity index (AI) were evaluated (refer to Fig. S3 in the Supporting Information for AI at all the study sites). AI was defined as the ratio of annual precipitation (*P*) to annual potential evapotranspiration (PET) and averaged over the observation period for each site (UNEP, 1992):

$$AI = \frac{P}{PET} \qquad (7)$$

The annual PET was determined by summing up the half-hourly PET values over the course of a year, using the United Nations Food and Agriculture Organization (FAO) Penman-Monteith method as outlined by Allen et al. (1998):

293 
$$PET = \frac{0.408\Delta(R_n - G) + \gamma \frac{900}{T_a + 273}u(e_s - e_a)}{\Delta + \gamma(1 + 0.34u)}$$
(8)

where  $\Delta$  is the slope of vapor pressure curve (kPa °C<sup>-1</sup>),  $R_n$  is the net radiation (MJ m<sup>-2</sup> hr<sup>-1</sup>), G is the soil heat flux density (MJ m<sup>-2</sup> hr<sup>-1</sup>),  $\gamma$  is the psychrometric constant (kPa °C<sup>-1</sup>),  $T_a$  is the air temperature (°C), u is the wind speed (m s<sup>-1</sup>),  $e_s$  is the saturation vapor pressure (kPa), and  $e_a$  is the actual vapor pressure (kPa). The estimation of AI is sensitive to gaps in precipitation data. Therefore, we used long-term mean annual precipitation provided on the site information page at

the FLUXNET website (https://fluxnet.org/sites/site-list-and-pages/) rather than calculating mean annual precipitation from the FLUXNET2015 dataset. For the sites where annual precipitation records were not provided, the high-frequency precipitation record in the FLUXNET2015 dataset was used.

303

304

305

306

307

308

309

310

311

312

313

314

315

316

317

318

319

320

321

302

299

300

301

### 2.4. Assessing the relationship between mWUE and IWUE

As a first step to conceptually understand the relationship between mWUE and IWUE, the relationship between IWUE and VPD was modeled by three hypothetical functions—linear, quadratic, and the Michaelis-Menten functions—based on the observations across the sites. The quadratic model of IWUE-VPD (hereafter IWUE<sub>0</sub>) depicts the case where IWUE increases with VPD until it reaches a maximum and then decreases afterward. In other words, when VPD is low, increasing IWUE with increasing VPD reflects a faster decrease of g<sub>s</sub> than A (due to the high intercellular  $CO_2$  concentration,  $c_i$ ), whereas decreasing IWUE with increasing VPD at high VPD reflects a faster decrease of A than  $g_s$  (low  $g_s$  at high VPD reduces  $c_i$  and eventually causes the steep decline of A). The linear model (hereafter IWUE<sub>L</sub>), on the other hand, represents a simplified IWUE-VPD relationship where IWUE would keep increasing with rising VPD assuming IWUE is only limited by  $g_s$  but not by photosynthetic capacity. The Michaelis-Menten function (hereafter IWUE<sub>M</sub>) represents the saturating IWUE under high VPD but does not account for IWUE reduction. Thus, the linear and quadratic functions are considered plausible "end members" describing the actual response of IWUE to VPD, while the Michaelis-Menten function is a more intermediate case. Mathematically, the IWUE<sub>L</sub>, IWUE<sub>M</sub>, and IWUE<sub>O</sub> take the forms:

$$IWUE_L = m VPD + n (9)$$

$$IWUE_{M} = \frac{IWUE_{max} \cdot VPD}{k + VPD} \tag{10}$$

323 
$$IWUE_{Q} = -a (VPD - b)^{2} + c$$
 (11)

where m is the slope of IWUE<sub>L</sub>, n is IWUE<sub>L</sub> at VPD = 0, IWUE<sub>max</sub> is the maximum potential IWUE, k is the VPD at which IWUE proceeds at half IWUE<sub>max</sub>, a represents the curvature of IWUE<sub>O</sub>, b is the vertex, c is the maximum IWUE<sub>O</sub> at the vertex.

The expected dynamics of mWUE across the FLUXNET sites in response to changing VPD were simulated based on an empirically driven IWUE-VPD model to understand how the mWUE metrics would respond to changing VPD and IWUE. To generate possible patterns of mWUE-VPD, the range of coefficients in the IWUE models was determined empirically from the data across the sites. To facilitate interpretation, the patterns were simulated by changing the curvature of the quadratic equation (Eq. 11), assuming the intercept is equal to zero. For the simulation of mWUE, a constant  $c_a$  was applied by calculating its average across the sites to focus on the interactions among VPD, IWUE, and mWUE (Eqs. 3 & 5).

Lastly, we investigated how IWUE (as a biological factor) and aridity index (as an environmental driver) influence the variability of mWUE. Based on the Eqs. 3 and 5, we hypothesized that a simple relationship between mWUE and the inverse of IWUE (IWUE<sup>-1</sup>) might emerge and would be affected by changing moisture conditions. Therefore, we identified a relationship between mWUE and IWUE<sup>-1</sup> for each study site and examined whether the relationship can be generalized across the sites based on the site-specific aridity index.

### 3. Results

## 3.1. Empirical response of IWUE to changing VPD or AI

To test the robustness of IWUE as a proxy of intrinsic water-use efficiency at the ecosystem level, we first compared the two different definitions of intrinsic water-use efficiencies at stand level, GPP divided by surface conductance ( $G_s$ ) (i.e., iWUE = GPP/ $G_s$ ) and inherent WUE (i.e., IWUE = GPP/ET×VPD/ $P_a$ ). The two WUE definitions were linearly correlated across the study sites (Fig. 1), and most sites had  $R^2$  values larger than 0.95 (Fig. 1b), indicating the robustness of IWUE as a proxy of intrinsic water-use efficiency at the ecosystem level (refer to the Supporting Information for an additional comparison of multiple definitions of intrinsic water-use efficiency; Figs. S1 & S2). We also performed the entire analysis using these two WUE definitions and observed similar results, which led to the same conclusion. Therefore, we only show the results from using IWUE hereafter.



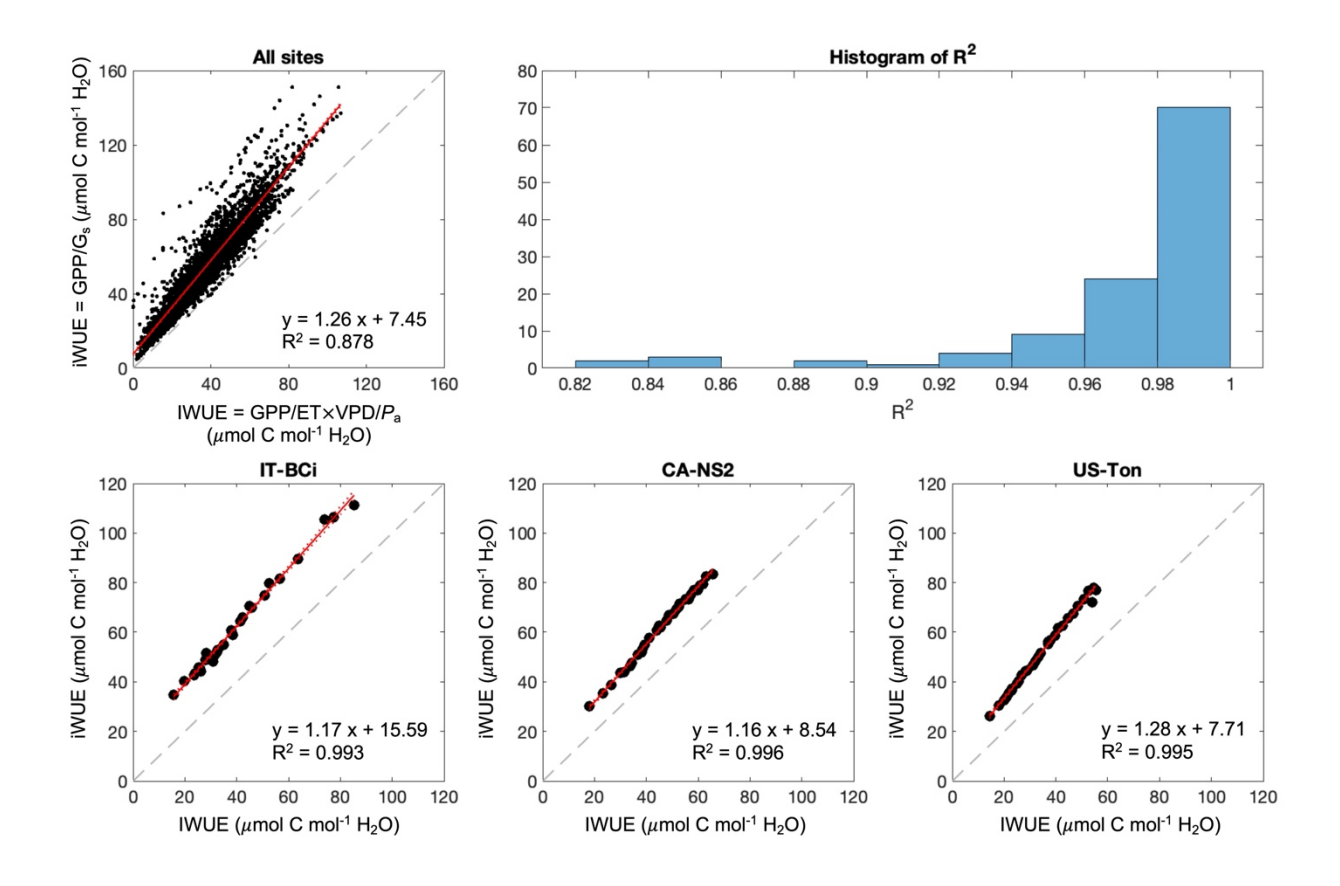
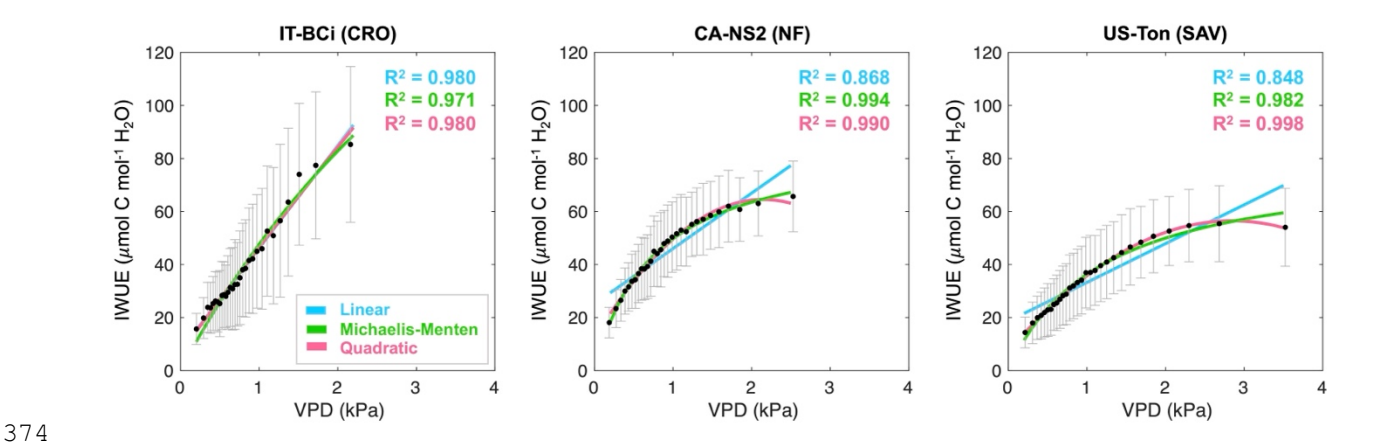


Figure 1. Comparison of two different definitions of water-use efficiencies at all sites (a) and at three sample sites (c, d, e): inherent water-use efficiency at the ecosystem level, IWUE (=  $GPP/ET \times VPD/P_a$ ), and intrinsic water-use efficiency at the ecosystem level, iWUE (=  $GPP/G_s$ ). Refer to Beer et al. (2009) for the comparison of different definitions of water-use efficiencies at leaf and ecosystem-level. Individual dots in panels a, c, d, and e indicate WUE partitioned into discrete bins spanning a range of VPD. Solid red lines indicate significant linear regressions (P < 0.05), and dashed red lines indicate 95% confidence interval. Dashed gray lines represent 1:1 lines. Panel b shows the histogram of coefficients of determination (R<sup>2</sup>) of the linear fits between IWUE and iWUE across the study sites.

In most cases, the Michaelis-Menten model and the quadratic model explained empirical IWUE patterns across the range of VPD better than the linear model (Fig. 2 and Fig. S3 in the Supporting Information). Specifically, the Michaelis-Menten model worked better for the sites where the increase of IWUE plateaued at high VPD, and the quadratic model worked better for the sites where IWUE started decreasing at very high VPD. On the other hand, the linear model often overestimated IWUE at low and high VPD, except the sites where IWUE-VPD was highly linear.



**Figure 2.** Examples of empirical (black dots) and modeled (linear: blue, Michaelis-Menten:

green, quadratic: red) responses of inherent water-use efficiency (IWUE) to changing vapor pressure deficit (VPD). The examples include three sites best represented by the linear model (IT-BCi, cropland), the Michaelis-Menten function (CA-NS2, needleleaf forest), and the quadratic model (US-Ton, savanna), respectively. Each error bar (light gray) represents the standard deviation of IWUE for each VPD bin (95% confidence). Refer to Fig. S4 in the Supporting Information for the IWUE-VPD relationships of all the study sites (n = 115).

When the site-specific IWUE-VPD slope values derived from the linear model (i.e., m in Eq. 9) were combined, we found increasing m with rising aridity index (P < 0.001, Fig. 3a). However, site-level aridity did not influence the intercept of IWUE-VPD relationship (P > 0.05, not shown here). When the sites were divided by their vegetation types, m increased with a rising aridity index in all vegetation types. However, the trend was only significant in grasslands,

croplands, and shrublands (P < 0.05, Fig. 3).

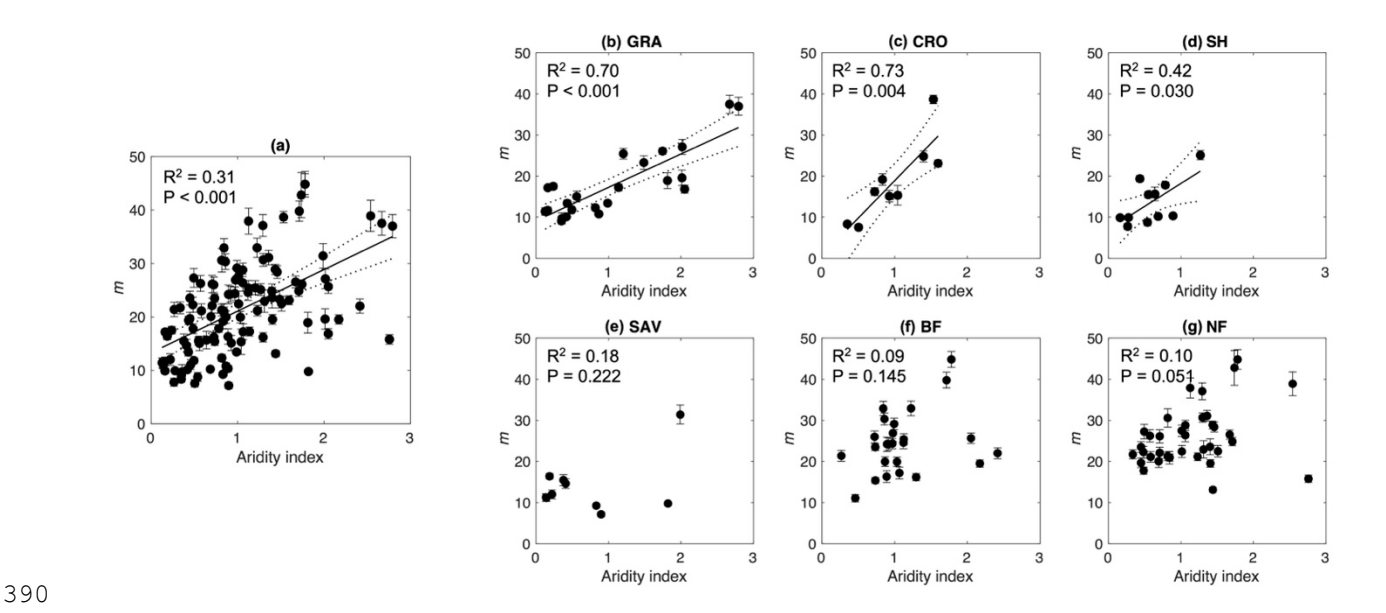


**Figure 3.** Relationship between the site-level aridity index and the regression slope of IWUE-VPD from individual sites (i.e., m in Eq. 9). Panel a shows the relationship when all sites were consolidated. The relationship is also illustrated separately for six different vegetation types in panels b to g (GRA: grassland, CRO: cropland, SH: shrubland, SAV: savanna, BF: broadleaf forest, NF: needleleaf forest). Each circle represents m from an individual site. Error bars represent standard errors of linear regressions. Solid lines indicate significant linear relationships (P < 0.05) and dashed lines indicate 95% confidence intervals.

## 3.2. Response of mWUE to changing VPD

Both of the mWUE indices,  $\partial E/\partial A$  and squared  $g_1$  ( $g_1^2$ ), showed a very similar response to changing VPD and indicated that the directional change of mWUE can be interpreted differently depending on the pattern of IWUE-VPD (Fig. 4). When the iWUE-VPD relationship is strongly linear, mWUE decreased exponentially and became less variable as VPD increased (Brighter curves in Figs. 4b & 4c). However, as the iWUE-VPD relationship became more non-

linear, mWUE declined at lower VPD and then increased at higher VPD (i.e., concave-up), rendering the mWUE-VPD relationship non-monotonic (darker curves in Figs. 4b & 4c).



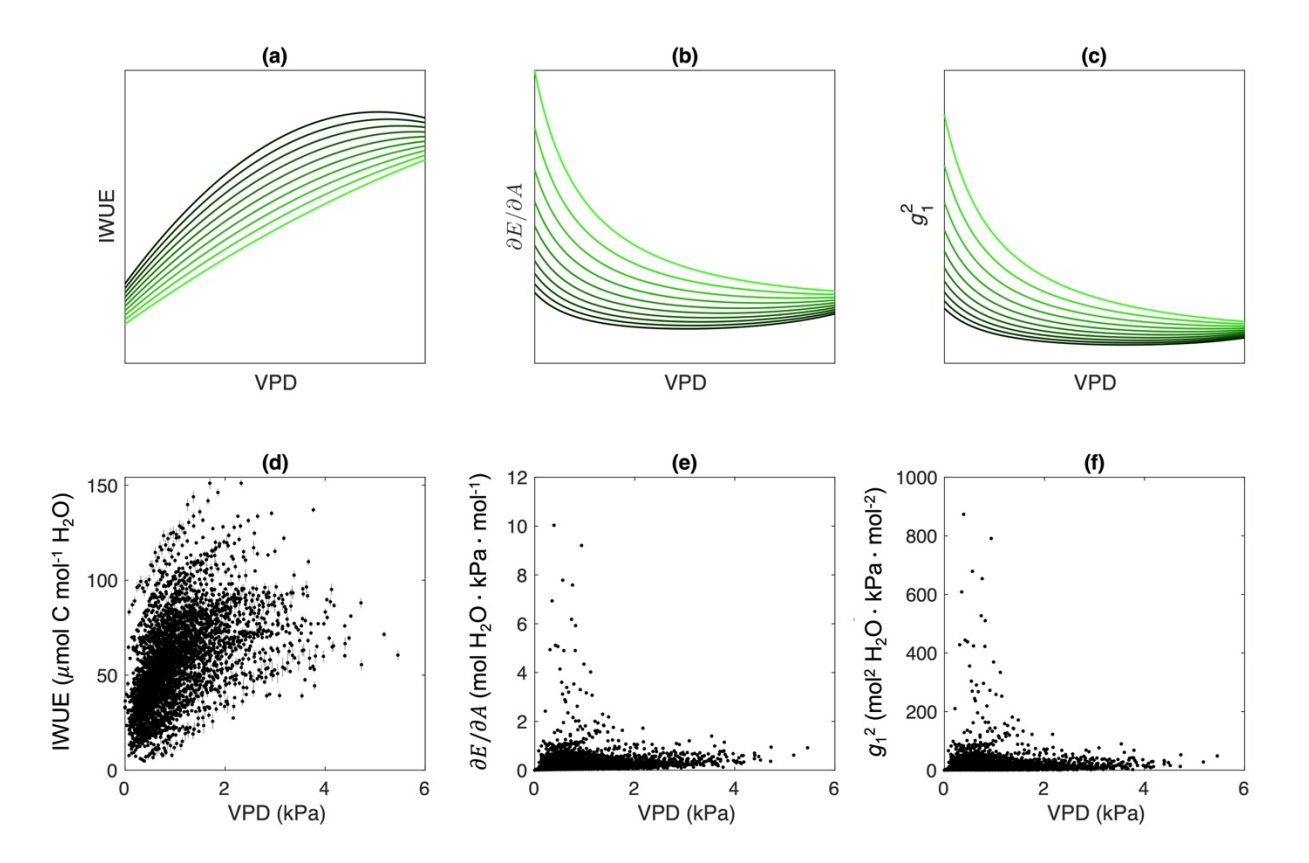


**Figure 4.** Hypothetical models of IWUE-VPD relationship (a), simulated  $\partial E/\partial A$ -VPD (b) and  $g_1^2$ -VPD (c) relationships based on typical cases, and their corresponding patterns illustrated using observations from all study sites (d, e, and f). The mWUE curves are the results of using the IWUE-VPD relationships of the corresponding colors. Note that IWUE-VPD relationships become more linear with lighter colors.

The simulated patterns of mWUE-VPD agreed well with the patterns from the empirical observation when the appropriate function for the IWUE-VPD relationship was applied. We show mWUE-VPD relationships from three study sites as examples (Fig. 5), of which IWUE-

VPD was represented best by linear, the Michaelis-Menten, and quadratic functions, respectively (refer to Fig. 2 for their corresponding IWUE-VPD relationships. Also, refer to Fig. S5 in the Supporting Information for the results of all study sites). As indicated by the simulation, the site with highly linear IWUE-VPD (IT-BCi) showed exponentially decreasing mWUE with rising VPD. In contrast, the other two sites with highly non-linear IWUE-VPD relationships had a concave-up pattern of mWUE-VPD. Notably, the mWUE-VPD relationship generated using a less optimal IWUE-VPD model can differ substantially from the empirical pattern. For example, application of linear IWUE-VPD function to the CA-NS2 and US-Ton, the sites represented best by the Michaelis-Menten and quadratic functions, respectively, generated concave-down mWUE-VPD pattern that is opposite to the actual pattern (Fig. 5). The disagreements between models and observations increased as VPD approached very high and very low extremes.



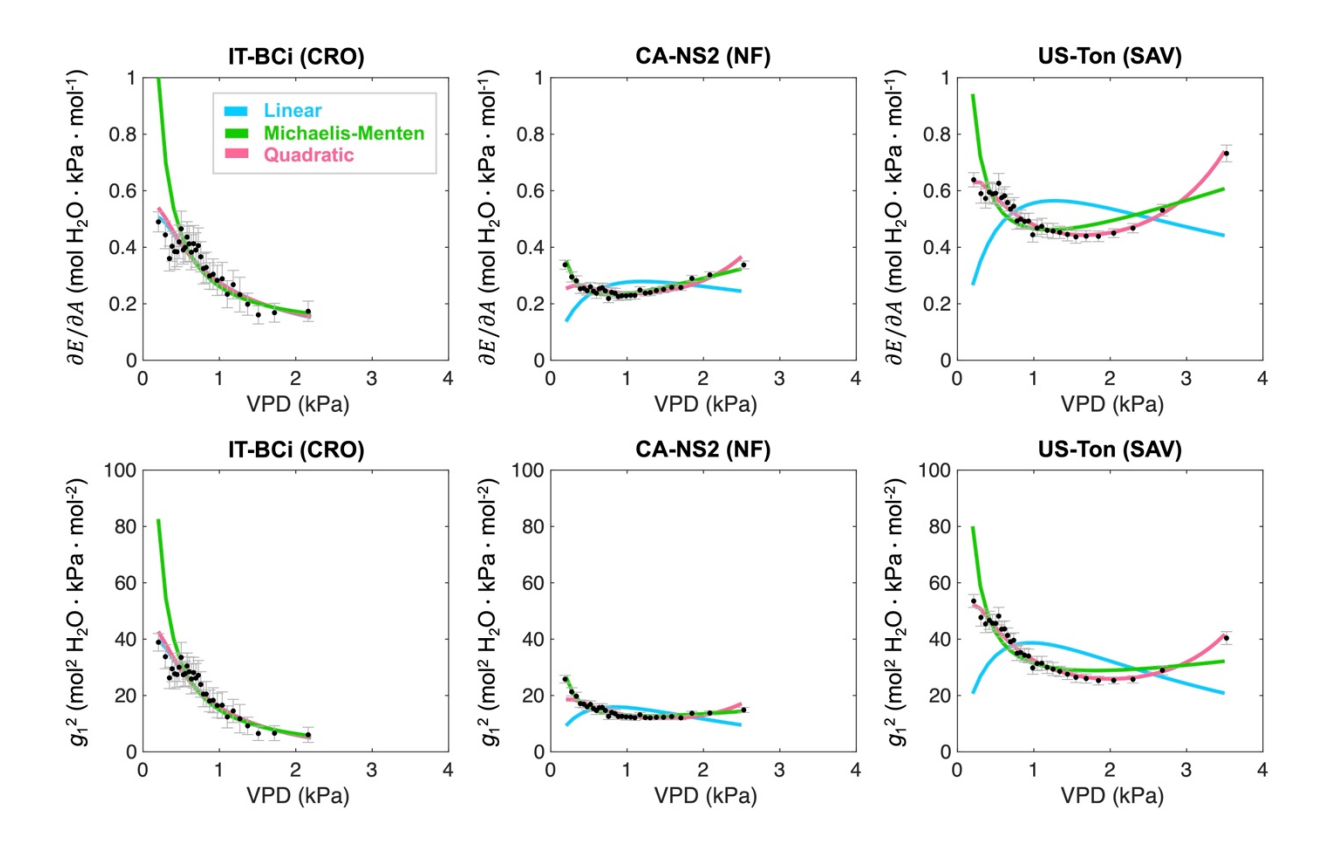
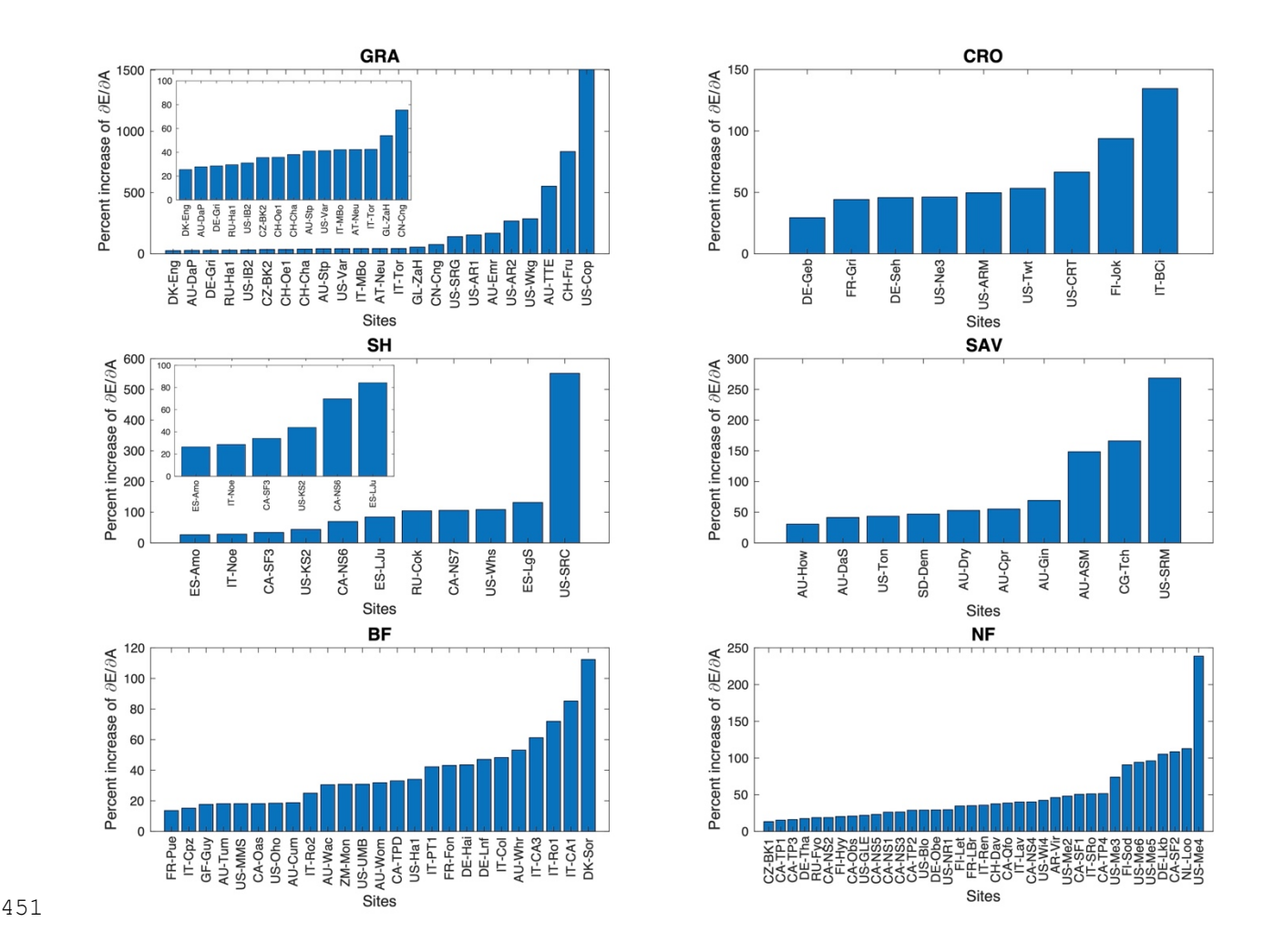


Figure 5. Examples of empirical (black dots) and modeled (linear: blue, Michaelis-Menten: green, quadratic: red) relationships between  $\partial E/\partial A$  (analytical solution by Katul et al., 2010) and vapor pressure deficit (VPD), and between  $g_1^2$  (Medlyn et al., 2012) and VPD. The examples include three sites best represented by the linear IWUE-VPD model (IT-BCi, cropland), the Michaelis-Menten function (CA-NS2, needleleaf forest), and the quadratic model (US-Ton, savanna), respectively. Note that the terms 'linear', 'Michaelis-Menten', and 'quadratic' denote the regression fits for the IWUE-VPD relationships (Refer to Fig. 2 for the IWUE-VPD relationships at the corresponding sites). Each error bar (light gray) represents the standard error of the mean IWUE for each VPD bin (95% confidence). Refer to Fig. S5 in the Supporting Information for the  $\partial E/\partial A$  -VPD relationships at the 115 study sites.

The variability of mWUE to changing VPD was substantial in most cases (Fig. 6). Out of the total of 115 study sites, the percent increase of  $\partial E/\partial A$  (i.e., growth in  $\partial E/\partial A$  from the lowest to the largest value at a site) was larger than 50% in 43 sites, and larger than 100% in 22 sites. Note that the reported percent increase was determined by excluding the upper and lower 10% of values. This step was taken to prevent exaggeration caused by extremely high  $\partial E/\partial A$  at low VPD, which is commonly observed across the study sites (refer to Figure S5 in the Supporting Information for the variability of  $\partial E/\partial A$  with VPD at all the study sites). As a result, the reported percent increase represents a conservative estimate overall.



**Figure 6.** Sorted percent increase of  $\partial E/\partial A$  (from the lowest  $\partial E/\partial A$ ) (GRA: grassland, CRO: cropland, SH: shrubland, SAV: savanna, BF: broadleaf forest, NF: needleleaf forest). Embedded plots in GRA and SH are zoomed in for those sites where percent increases are lower than 100%. Note that the percent increases were calculated after removing values of the highest 10% and lowest 10% to avoid exaggeration due to very high  $\partial E/\partial A$  at low VPD at some sites. Therefore, the reported percent increase values are conservative estimates for most sites.

### 3.3. Correlation between mWUE and IWUE

Although the trend of mWUE-VPD seems hard to generalize, the simulated mWUE had a clear linear relationship with IWUE<sup>-1</sup> for the majority of IWUE's range regardless of the linearity

of the IWUE-VPD relationship except when IWUE is very high (i.e., under high VPD, Fig. 7). Although limited to a small portion of the entire range, a sharp directional change in the variation of mWUE was near a point where IWUE<sup>-1</sup> was smallest, and strong linearities between mWUE and IWUE<sup>-1</sup> were found before and after the transitional point. Substantial hysteresis became more evident as the IWUE-VPD pattern became more curved (darker curves in Fig. 4).

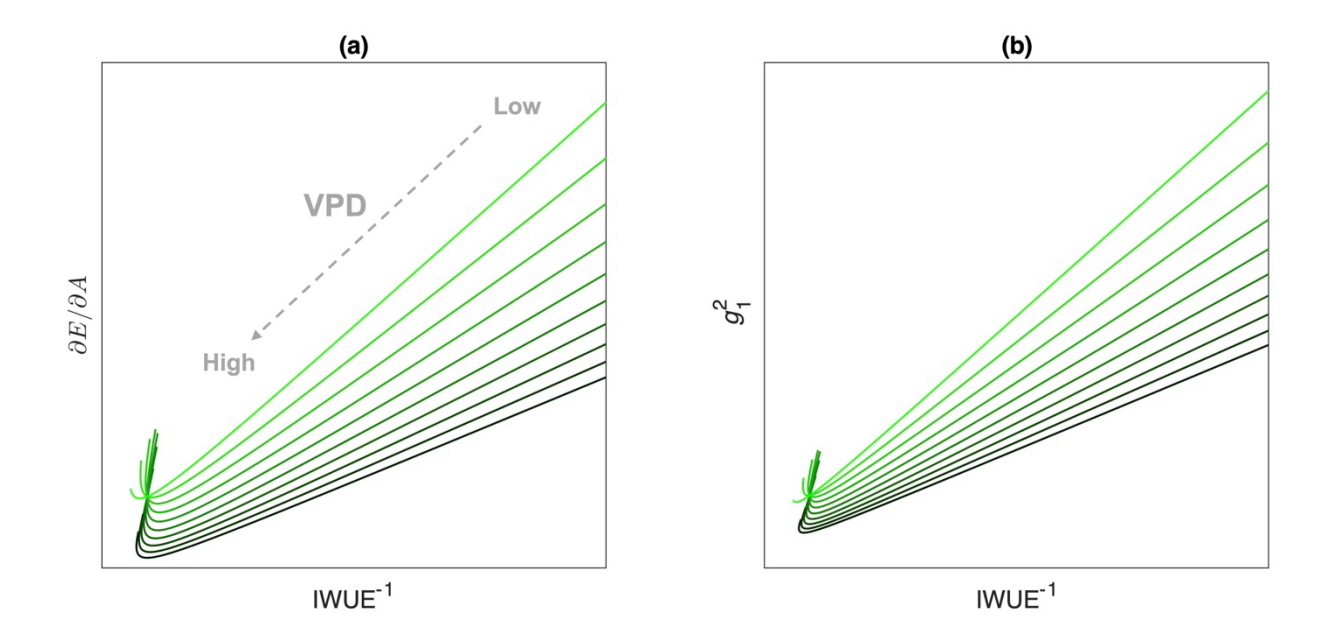


**Figure 7.** Simulated relationship between mWUE metrics ( $\partial E/\partial A$  and  $g_1^2$ ) and IWUE-1 (based on the hypothetical IWUE-VPD model in Fig. 4). The colors of the curves correspond to those used in Fig. 4: IWUE-VPD relationships become more linear with lighter colors. Dashed arrows in panel a represent the directional change of VPD from low to high VPD.

As predicted by the simulated mWUE-IWUE<sup>-1</sup> relationships (Fig. 7), the empirical mWUE-IWUE<sup>-1</sup> relationship was strongly linear (P < 0.001 at all sites, Fig. 8). A sign of hysteresis was noticeable for the site that showed decreasing iWUE under very high VPD (US-

Ton, refer to Fig. 2 for its IWUE-VPD relationship). In contrast, hysteresis was less evident at the other sites. When the relationship was drawn by grouping data by different levels of IWUE (black dots in Fig. 8), hysteresis was not observed, and the mWUE-IWUE<sup>-1</sup> relationship was strongly linear.



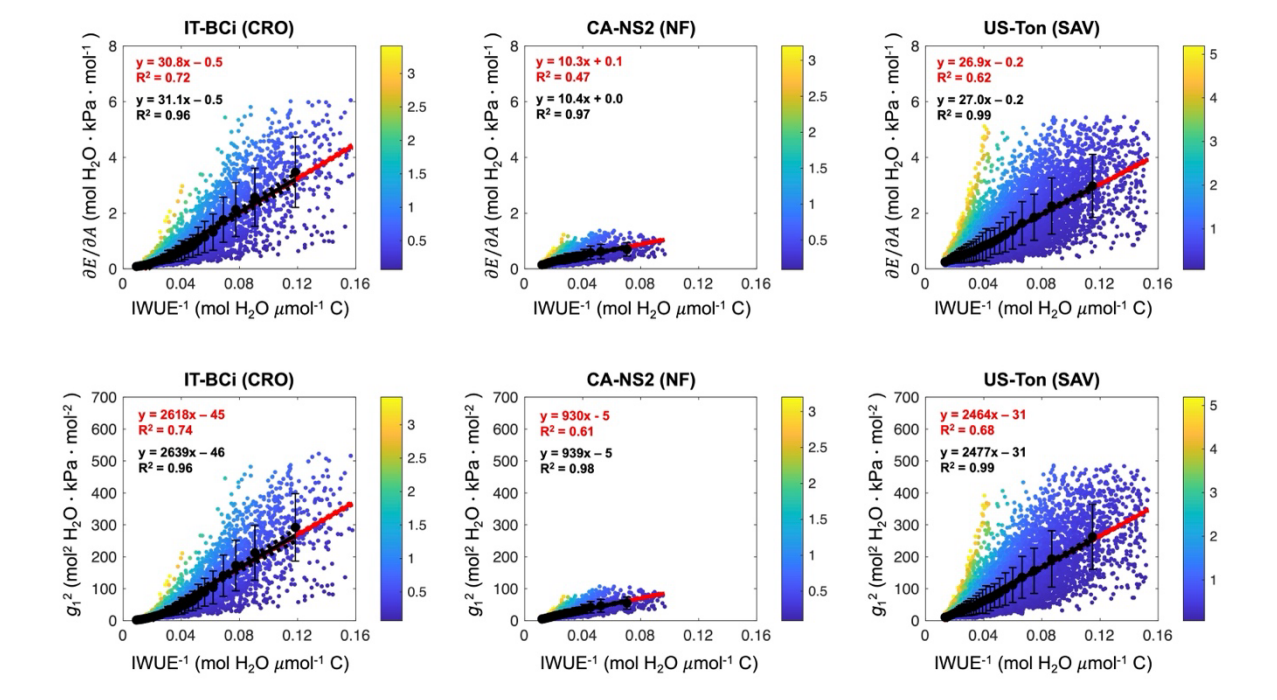
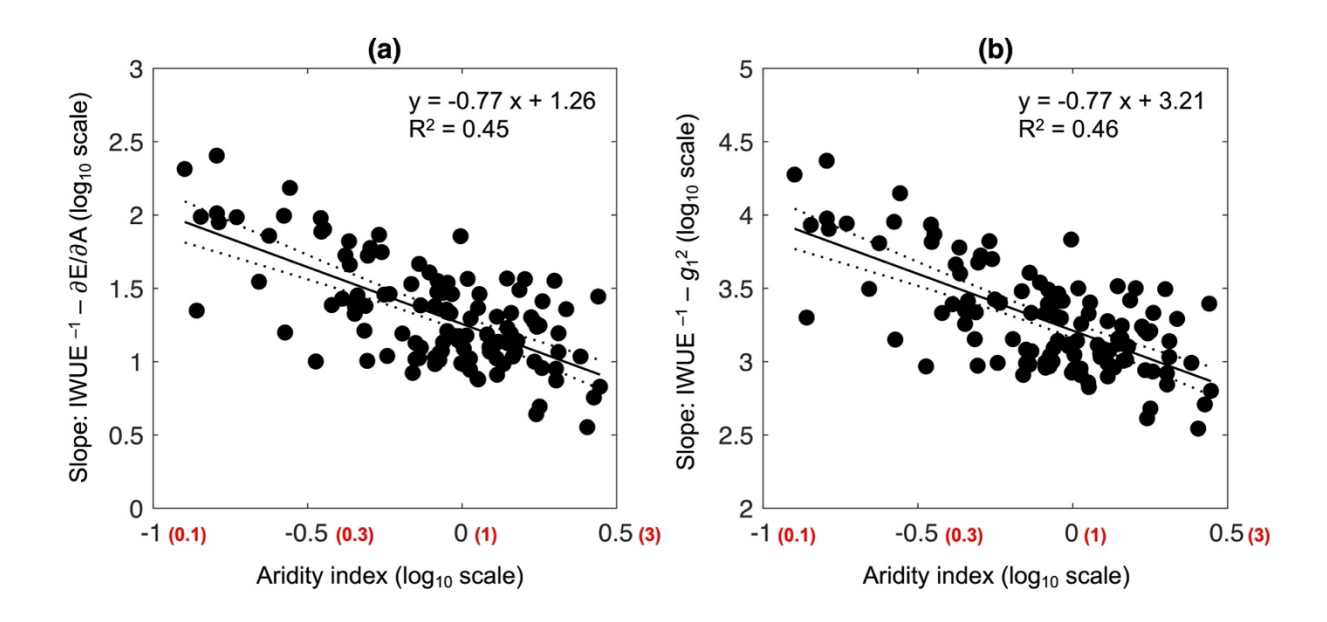


Figure 8. Examples of empirical relationship between mWUE metrics ( $\partial E/\partial A$  and  $g_1^2$ ) and IWUE-<sup>1</sup>. The examples include three sites best represented by the linear IWUE-VPD model (IT-BCi, cropland), the Michaelis-Menten function (CA-NS2, needleleaf forest), and the quadratic model (US-Ton, savanna), respectively. Refer to Fig. 2 for the IWUE-VPD relationships at the corresponding sites. Colorful dots represent hourly data points shaded based on the level of VPD (refer to color bars for the scale of VPD). Black dots represent data binned by IWUE-<sup>1</sup>: Data binning was performed to distribute sample sizes evenly across bins (~30 samples per bin). Error bars represent standard deviations. The red and black solid lines indicate linear fits for hourly and binned data, respectively. Dashed red lines represent confidence intervals for the slopes of linear regressions. Note that red and black linear regressions and their confidence intervals overlap. Refer to Fig. S6 in the Supporting Information for the  $\partial E/\partial A$  - IWUE-<sup>1</sup> relationships at the 115 study sites.

We investigated whether the relationship between mWUE and IWUE<sup>-1</sup> could be generalized across the sites based on the site-specific AI. Specifically, the linear IWUE<sup>-1</sup>-mWUE slopes (hereafter  $m^*$ ) from all study sites were merged, and their variability in response to changing AI was evaluated. We found a significant linear relationship between  $m^*$  and AI when both are scaled by  $\log_{10}$  (P < 0.001, Fig. 9). The  $m^*$  was larger at the drier sites (i.e., sites of lower AI) than at the wetter sites (i.e., sites of larger AI). However, we did not find a significant relationship between the IWUE<sup>-1</sup> – mWUE intercept and AI (P > 0.05, not shown here).



**Figure 9.** Relationships between IWUE<sup>-1</sup>-mWUE slope and aridity index (= P/PET) derived from all the study sites (n = 115). Each circle represents the slope obtained from an individual site. Both the x and y axes are scaled by  $\log_{10}$ . The numbers in parentheses next to the x-axis tick labels represent the aridity indices before the log transformation. The solid lines indicate linear regressions, and the dashed lines indicate confidence intervals (95% confidence interval).

We further tested whether we could find the similar relationship when the sites were grouped by the vegetation type. We found decreasing  $m^*$  with rising AI in grasslands, croplands, and shrublands (P < 0.01, Fig. 10). On the other hand,  $m^*$  was relatively constant across the range of AI in savannas, deciduous broadleaf forests, and evergreen needleleaf forests (P > 0.05, Fig. 10).

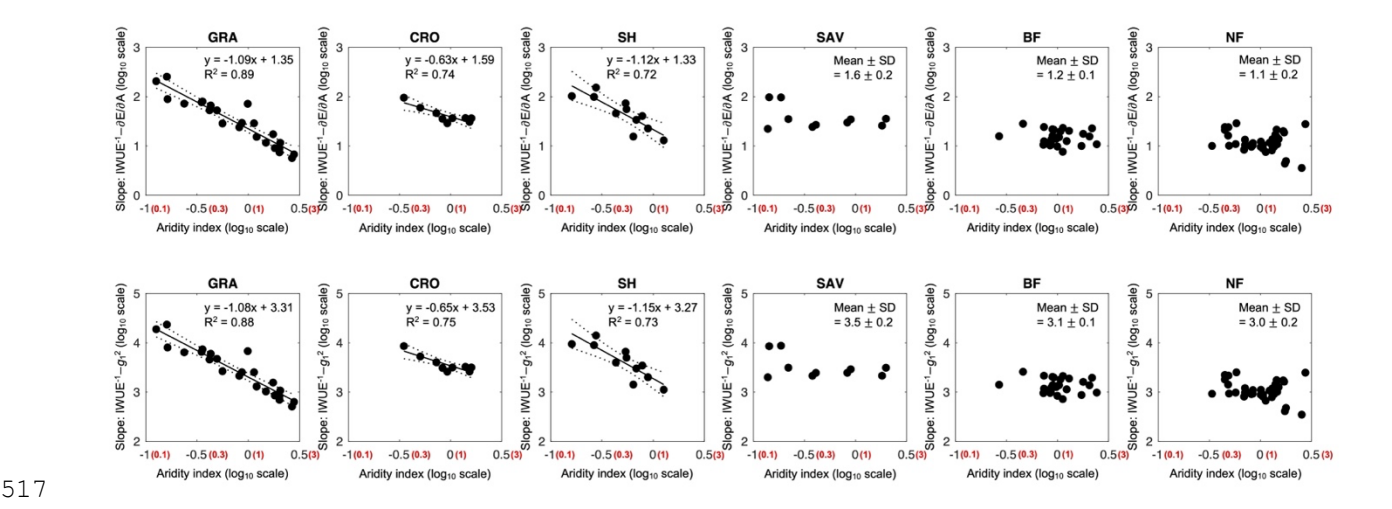


**Figure 10.** Relationships between log-transformed IWUE<sup>-1</sup>-mWUE slope and aridity index in different vegetation types (GRA: grassland, CRO: cropland, SH: shrubland, SAV: savanna, BF: broadleaf forest, NF: needleleaf forest). Each circle represents the log-transformed slope obtained from an individual site. The numbers in parentheses next to the x-axis tick labels represent the aridity indices before the log transformation. Solid lines indicate significant linear relationships (P < 0.05), and dashed lines indicate 95% confidence intervals.

## 4. Discussion

Stomatal optimization theory, which originated with the work of Cowan and Farquhar (1977), has experienced a recent surge in popularity as the vegetation modeling community continually seeks ways to inject more theoretical rigor into Earth system models (Anderegg et al., 2018; Bassiouni & Vico, 2021; Bonan et al., 2014; Feng et al., 2022; Katul et al., 2010; Katul et al., 2009; Lin et al., 2018; Lin et al., 2015; Lu et al., 2020; Lu et al., 2016; Medlyn et al., 2012, 2017; Novick et al., 2016b; Sabot et al., 2022; Sperry et al., 2017; Wolf et al., 2016). The marginal water-use efficiency (mWUE) is a key parameter in this type of model, but we still need a clear understanding of how mWUE is regulated biologically and environmentally. Lin et

al. (2018) previously suggested suboptimal mWUE in response to VPD at a sub-daily scale by estimating site-specific, best-fitted exponent for VPD based on the variation model of optimality theory (Medlyn model), which inspired our study. In comparison, our study is unique in analyzing the dynamics of mWUE observed at the half-hourly timescale in response to changing VPD owing to the long-term continuous carbon and water flux data from the network of eddy covariance towers.

Another motivation for our study was the conflicting arguments over the dynamics of mWUE in response to water stress. Although mWUE is in general considered to be nearly constant during a day under stable soil moisture conditions (Berninger & Hari, 1993; Fites & Teskey, 1988; Hall & Schulze, 1980; Hari et al., 2000), several studies showed that mWUE changed with different levels of water stress. For example, theoretical considerations indicate a monotonic decrease of mWUE with higher water stress when the stochasticity of rainfall depths is neglected (Cowan, 1982; Makela et al., 1996), although some empirical estimates showed that mWUE increases under severe water stress (Farquhar et al., 1980b; Grieu et al., 1988). On the other hand, Manzoni et al. (2011) performed a meta-analysis of 50 species to estimate mWUE from gas exchange observations along gradients of soil moisture and showed that mWUE decreases under mild water stress but increases under severe water stress (note that they defined  $\lambda = \partial A/\partial E$ , which is inverse of the definition used by Cowan & Farquhar (1977) and this study).

### 4.1. Relationship between IWUE and VPD

Based on the two equations of stomatal optimization theory (Eqs. 3 & 5), we first characterized the variability of mWUE based on the relationship between IWUE and VPD,

representing biological and environmental factors, respectively. We show that the variability of IWUE needs to be modeled accurately to emulate the variability of mWUE in response to water stress correctly. For example, as demonstrated in Fig. 5 (CA-NS2 & US-Ton), oversimplifying the IWUE-VPD relationship by modeling it with a linear function can incorrectly interpret mWUE variability.

557

558

559

560

561

562

563

564

565

566

567

568

569

570

571

572

573

574

575

576

577

578

579

The non-linear IWUE-VPD relationship is presumably driven by different rates of carbon assimilation and water loss in response to changing VPD at an hourly scale, reflecting the balance between stomatal and non-stomatal limitations to photosynthesis at the leaf level (Farquhar, 1978; Jones, 2014). Under low to moderate VPD conditions, photosynthesis is less sensitive to changing intercellular CO<sub>2</sub> concentration because stomatal conductance is high enough to maintain the high intercellular CO<sub>2</sub> when VPD is low to moderate. Therefore, the quantity of reduced water loss by stomatal closure (ET at an ecosystem level) outweighs the quantity of reduced carbon assimilation (GPP at an ecosystem level) when VPD rises (i.e.,  $|\Delta GPP| < |\Delta ET|$ ), resulting in the increasing phase of IWUE. As VPD keeps increasing, photosynthesis can be limited when the reduction of stomatal conductance under high VPD conditions substantially reduces intercellular CO<sub>2</sub> concentration (i.e.,  $|\Delta GPP| \approx |\Delta ET|$ ), resulting in the steady phase of IWUE. As VPD becomes excessively high, photosynthesis will be further suppressed by high temperature (Yamori et al., 2014) and low leaf water potential (Lawlor & Tezara, 2009) that are associated with dry conditions (i.e.,  $|\Delta A| > |\Delta g_s|$ ), leading to the decreasing phase of IWUE.

Therefore, assuming a linear IWUE-VPD relationship may not only fail to emulate observations but also oversimplify the physiological responses to water stress. Our analysis recommends using the Michaelis-Menten function for most sites while utilizing a quadratic

function for sites exhibiting extreme cases where IWUE declines under high VPD conditions. The Michaelis-Menten function can be beneficial to characterize the IWUE-VPD relationship because the maximum potential IWUE and the rate of IWUE increase can be identified during parameterization (Eq. 10). Although the quadratic function can emulate IWUE-VPD relationships very well or performs even better than the Michaelis-Menten function in some cases where IWUE decreases at high VPD, it is parameterized empirically and as a result, lacks mechanistic information. Nevertheless, the quadratic function is preferable to the linear function.

580

581

582

583

584

585

586

587

588

589

590

591

592

593

594

595

596

597

598

599

600

601

602

It is also important to consider the definition of water-use efficiency for accuracy. We used inherent water-use efficiency (IWUE) as a proxy of intrinsic water-use efficiency (iWUE) at the ecosystem level as suggested by Beer et al. (2009), which can be estimated by GPP and ET inferred from the flux tower observations. This approximation is particularly useful over a more common ecosystem-level iWUE =  $GPP/G_s$  because IWUE requires fewer variables and is easier to extrapolate to a larger scale. However, it is important to note that ET/VPD in the equation of IWUE (Eq. 6) is a proxy of canopy conductance, assuming the canopy is well coupled to the atmosphere, boundary layer resistance is small, and thermal equilibrium between leaf and air is achieved (Beer et al., 2009). In other words, IWUE under non-equilibrium between canopies and atmosphere can be overestimated due to the higher VPD than the vapor pressure gradient near the canopy surface (i.e., the difference between intercellular vapor pressure  $(e_i)$  and atmospheric vapor pressure  $(e_a)$ ,  $e_i - e_a$ ). Difference between leaf and air temperature can also influence the  $e_i$  $-e_a$ ; if leaf temperature is higher than air temperature (as it often is, e.g., Novick & Barnes, 2023; Yi et al., 2020),  $e_i$  will increase while  $e_a$  remains constant, resulting in larger  $e_i - e_a$  than measured VPD and consequently underestimate IWUE. Therefore, it is important to address this potential bias to quantify iWUE accurately. According to our results, the correlation between the

two ecosystem-level iWUE proxies was strong at the site level (Fig. 1), implying that the choice of ecosystem-level iWUE definition is unlikely to influence our interpretation of the iWUE and mWUE variabilities substantially. Furthermore, our comparison of multiple definitions of iWUE using a mechanistic model, CANVEG (refer to the Supporting Information for more details), indicated that IWUE is a good proxy of leaf-level iWUE and meets the general assumptions to address scaling issues. Thus, we conclude that eddy covariance observation of carbon and water fluxes is suitable to model the variability of intrinsic water-use efficiency in response to changing VPD.

Of note, the linear relationship between the slope of IWUE-VPD and aridity index (Fig. 4) was stronger in the ecosystems characterized by lower vegetation types (e.g., grasslands, croplands, and shrubland). In contrast, ecosystems with higher vegetation (e.g., savannas, broadleaf forests, and needleleaf forests) exhibited a weaker relationship. This observation implies a potential link between water-use efficiency and the vertical structure of vegetation, although the exact underlying mechanism remains uncertain.

### 4.2. Modeling the variability of mWUE

We compared two solutions of mWUE by Katul et al. (2010) ( $\partial E/\partial A$ ) and Medlyn et al. (2012) ( $g_1$ ) developed based on different assumptions on stomatal optimality (carbon-limited versus light-limited) for more robust conclusion. Despite the difference in the assumption, both solutions yielded very similar results throughout our analysis, confirming that the optimality assumption had little effect on evaluating the variability of mWUE in response to changing moisture conditions.

We characterized the trend of mWUE by using VPD as an environmental driver (Figs. 4 & 5), where its variability in response to VPD was unique and not necessarily unidirectional, thus making it hard to generalize with commonly available functions. Specifically, the variability of mWUE was simpler and decreased exponentially with rising VPD when the IWUE-VPD relationship was more linear, making it easy to model the mWUE-VPD relationship (Figs. 4 & 5). However, the variability of mWUE was not unidirectional when the IWUE-VPD relationship was non-linear, as observed in most cases (Fig. S5 in the Supporting Information); high variability in mWUE is usually observed at low- and high-ends of VPD. On the other hand, when mWUE was calculated under conditions of moderate VPD level only, the variability of mWUE can be overlooked and considered constant. This complex pattern signifies the importance of a comprehensive view of IWUE and mWUE across the full potential range of VPD. Observation under conditions of a partial range of environmental factors is common in many types of field measurements that have coarser time resolution (hourly versus daily to weekly, e.g., eddy covariance versus leaf gas exchange measurements) unless they are performed frequently over a long period to cover non-typical conditions. We were able to estimate precise variability of mWUE matching with the hypothetical models owing to the large amount of data (FLUXNET2015) collected every half-hour over the long period throughout the network of flux towers (total 1,036 site years with many sites offering data collected over more than a decade), highlighting the value of long-term, continuous measurements. Overall, our result of the mWUE-VPD relationship supports the results of Manzoni et al. (2011) among the various conflicting results over the response of mWUE in response to water stress, which found decreasing mWUE under mild water stress and increasing mWUE under severe water stress from a meta-analysis of gas exchange observations.

625

626

627

628

629

630

631

632

633

634

635

636

637

638

639

640

641

642

643

644

645

646

As a solution to model unique patterns of mWUE, we attempt to address its variability with information that can be obtained easily from various types of field measurements (e.g., eddy covariance, gas exchange, and tree-ring cores) and modeled empirically—IWUE. The relationship between mWUE and IWUE was inferred from the two equations of the optimization theory (Eqs. 3 & 5). We found a strong linear correlation between IWUE-1 and mWUE from both empirical data (Fig. 8) and modeling exercise (Fig. 7). In other words, the variability of mWUE in response to changing VPD can be characterized by (1) the function of IWUE-VPD relationship and (2) the slope between IWUE-1 and mWUE. The relationship between IWUE-VPD is relatively simple and can be identified with various field measurements. This raises the question of whether a simple way exists to identify the slope between IWUE-1 and mWUE. By synthesizing the IWUE-1-mWUE slopes across the sites, we found that the IWUE-mWUE slope is highly correlated with the site-specific AI that can be characterized for different vegetation types (Fig. 9). The correlation is conceivable from the equations of mWUE (Eqs. 3 & 5). If, for instance, Eq. 3 is rearranged,

$$\frac{\partial E/\partial A}{\text{IWUE}^{-2}} \propto \text{VPD} \qquad (12)$$

indicating that the slope between mWUE and the inverse of IWUE is proportional to VPD, which is commensurate with AI at a site-level. The correlation between the IWUE<sup>-1</sup>-mWUE slope and the AI at a site level implies that the aridity index is a good surrogate for the site-specific IWUE<sup>-1</sup>-mWUE slope.

We further illustrated how the correlations between the IWUE<sup>-1</sup>-mWUE slope ( $m^*$ ) and AI vary across vegetation types (Fig. 10). Among the vegetation types, GRA, CRO, and SH had strong correlations between  $m^*$  and AI, which indicated that using different  $m^*$  depending on the site-level dryness would be appropriate. On the other hand, the low variability of  $m^*$  observed in

SAV, BF, and NF indicates that constant  $m^*$  can generate a reasonably accurate mWUE-VPD relationship regardless of the site-level dryness. Although the reasons for this difference are not entirely clear, this empirical relationship can help more accurately model the variability of mWUE in response to changing VPD across the sites and biomes. Growth in data availability across the flux tower network helps ensure the coverage of the full potential range of environmental factors. More data availability can be achieved by consistently collecting good-quality data from existing study sites and establishing new sites in underrepresented areas. Furthermore, additional data would also help the development of  $m^*$  in detail, for instance, based on the plant water-use strategies, with the aid of conjoined field measurements such as water potential  $(\Psi)$  of soil and plant.

## 4.3. Implications for future research

It is important to note that plant response to water stress is not only determined by the water demand (i.e., atmospheric dryness or VPD) but also by the availability of water sources (i.e., soil moisture). Although volumetric soil moisture content ( $\theta$ ) is often considered as a metric of soil water available to plants, soil water potential ( $\Psi_S$ ) is the driving force of water flows that becomes available to plants by moving along gradients of water potential through the plant (stem and leaf) and eventually to the air. Moreover,  $\Psi_S$  is not only determined by the  $\theta$  but also by soil physical properties, and thus can differ even under conditions of the same  $\theta$  (Campbell, 1974; van Genuchten, 1980). Unlike  $\Psi_S$ ,  $\theta$  is widely measured and usually available with flux data, and carbon and water fluxes are often explained as a function of  $\theta$  (Green et al., 2019; Novick et al., 2016a). However,  $\theta$  may not characterize soil moisture availability to plants properly, and its relationship with carbon and water fluxes is usually nonlinear and threshold-driven (Feldman et

al., 2019; Novick et al., 2022; Stocker et al., 2018), making the modeling of the relationship between IWUE and soil moisture availability challenging. Therefore, enhanced accessibility to  $\Psi_S$  data by improving the ease and reliability of  $\Psi_S$  observations, for example, by building a centralized and standardized network of  $\Psi$  (Novick et al., 2022) would be a necessary step to better characterize the effect of soil moisture availability on plant responses such as IWUE and mWUE.

694

695

696

697

698

699

700

701

702

703

704

705

706

707

708

709

710

711

712

713

714

715

716

In this study, we tested the two stomatal optimization models (Katul et al., 2010; Medlyn et al., 2012) that are elaborations of the original Cowan & Farquhar (1977) model with few modifications because our goal was to characterize variability of mWUE in response to dryness (VPD and aridity index) using IWUE that can be calculated from the extensive, long-term continuous data from the network of eddy covariance. Meanwhile, more recent optimization models are incorporating additional physiological penalties than the water loss, for instance, damage to the vascular system induced by water stress (Anderegg et al., 2018; Sperry et al., 2017; Wolf et al., 2016), which may enhance prediction of long-term plant responses to climate change. Although monitoring the integrity of the vascular system, which can be informed by the dynamics of hydraulic conductivity, has not been widely conducted, recent advances in psychrometric approaches allowing continuous measurements of plant  $\Psi$  (e.g., PSY1 manufactured by ICT International) and  $\Psi_S$  (e.g., TEROS 21 manufactured by Meter Group) are now enabling the monitoring the dynamics of hydraulic conductivity. Moreover, the relationship between plant and soil  $\Psi$  can be used to identify plant water-use strategies (e.g., isohydry framework; Martinez-Vilalta et al., 2014), which can help develop  $m^*$  based on plant water-use strategies. The measurements of carbon and water fluxes using the eddy covariance technique with the aid of the centralized and standardized deployment of  $\Psi$  sensors (Novick et al., 2022)

will have a great potential to test models and theories of stomatal optimization and advance our knowledge of it.

## **Acknowledgments**

We thank FLUXNET/AmeriFlux community for managing their sites, collecting and processing data, and making data available to public and broader scientific community. K.Y. and G.B.S. acknowledge support from the NSF Division of Earth Sciences (Grant # 2012893) through CUAHSI and the U.S. Geological Survey (USGS) John Wesley Powell Center for Analysis and Synthesis. K.A.N and T.H. were supported by the NASA Carbon Science Program (Grant # NNX17AE69G). K.A.N. also acknowledges support from the NSF Division of Environmental Biology (Grant # 1552747), the NSF Division of Integrative Organismal Systems (Grant #2006196), and the AmeriFlux Management Project. L.W. was supported by the NSF Division of Earth Sciences (Grant # 1554894). X.Y. was supported by the NSF Division of Integrative Organismal Systems (Grant # 2005574). K.M. was supported by the INTER Mobility Fellowship from the FNR Luxembourg (INTER/MOBILITY/2020/14521920/MONASTIC). This article has been peer reviewed and approved for publication consistent with USGS Fundamental Science Practices.

## **Author Contributions**

K.Y., K.A.N., and D.B. conceptualized the research and developed the methodology.

K.Y., D.B., and M.B. analyzed the data, and K.A.N, Q.Z., L.W., T.H., X.Y., K.M., and G.B.S. validated the analysis. K.Y. visualized the data analysis. K.Y. wrote the manuscript with input and revisions from all authors.

740	
741	Conflict of Interest
742	The authors declare that they have no conflict of interest.
743	
744	Data Availability
745	The data that support the findings of this study are openly available in the FLUXNET
746	Data Portal at https://fluxnet.org/data/fluxnet2015-dataset/. The list of DOIs for the individual
747	FLUXNET sites used in this study is available in the Supporting Information (Table S1).
748	
749	References
750	Allen, R. G., Pereira, L. S., Raes, D., & Smith, M. (1998). Crop evapotranspiration-Guidelines
751	for computing crop water requirements-FAO Irrigation and drainage paper 56. FAO,
752	Rome, 300(9), D05109.
753	Ammann, C. (2002-2008). FLUXNET2015 CH-Oe1 Oensingen grassland [Dataset]. FLUXNET
754	https://doi.org/10.18140/FLX/1440135
755	Anderegg, W. R. L., Wolf, A., Arango-Velez, A., Choat, B., Chmura, D. J., Jansen, S., Kolb, T.
756	Li, S., Meinzer, F. C., Pita, P., de Dios, V. R., Sperry, J. S., Wolfe, B. T., & Pacala, S.
757	(2018). Woody plants optimise stomatal behaviour relative to hydraulic risk. <i>Ecology</i>
758	Letters, 21(7), 968–977. https://doi.org/10.1111/ele.12962
759	Anderegg, W. R. L., Wolf, A., Arango-Velez, A., Choat, B., Chmura, D. J., Jansen, S., Kolb, T.
760	Li, S., Meinzer, F., Pita, P., de Dios, V. R., Sperry, J. S., Wolfe, B. T., & Pacala, S.
761	(2017). Plant water potential improves prediction of empirical stomatal models. PLoS

One, 12(10), e0185481. https://doi.org/10.1371/journal.pone.0185481

Ardö, J., Tahir, B., & Elkhidir, H. (2005-2009). FLUXNET2015 SD-Dem Demokeya 763 [Dataset]. FLUXNET. https://doi.org/10.18140/FLX/1440186 764 Arndt, S., Hinko-Najera, N., Griebel, A., Beringer, J., & Livesley, S. (2010-765 2014). FLUXNET2015 AU-Wom Wombat [Dataset]. FLUXNET. 766 https://doi.org/10.18140/FLX/1440207 767 768 Aurela, M., Tuovinen, J. P., Hatakka, J., Lohila, A., Mäkelä, T., Rainne, J., & Lauria, T. (2001-2014). FLUXNET2015 FI-Sod Sodankyla [Dataset]. FLUXNET. 769 https://doi.org/10.18140/FLX/1440160 770 Baldocchi, D. D., & Harley, P. C. (1995). Scaling carbon dioxide and water vapour exchange 771 from leaf to canopy in a deciduous forest. II. Model testing and application. *Plant, Cell &* 772 Environment, 18(10), 1157–1173. https://doi.org/10.1111/j.1365-3040.1995.tb00626.x 773 Baldocchi, D., & Meyers, T. (1998). On using eco-physiological, micrometeorological and 774 biogeochemical theory to evaluate carbon dioxide, water vapor and trace gas fluxes over 775 776 vegetation: A perspective. Agricultural and Forest Meteorology, 90(1), 1–25. https://doi.org/10.1016/S0168-1923(97)00072-5 777 Baldocchi, D. D., Keeney, N., Rey-Sanchez, C., & Fisher, J. B. (2022). Atmospheric humidity 778 779 deficits tell us how soil moisture deficits down-regulate ecosystem evaporation. Advances in Water Resources, 159, 104100. https://doi.org/10.1016/j.advwatres.2021.104100 780 781 Ball, J. T., Woodrow, I. E., & Berry, J. A. (1987). A Model Predicting Stomatal Conductance 782 and its Contribution to the Control of Photosynthesis under Different Environmental Conditions. In: Biggins, J. (Ed.), *Progress in Photosynthesis Research*. pp. 221–224. 783 Springer, Dordrecht. https://doi.org/10.1007/978-94-017-0519-6 48 784

Bassiouni, M., & Vico, G. (2021). Parsimony vs predictive and functional performance of three 785 stomatal optimization principles in a big-leaf framework. New Phytologist, 231(2), 586-786 600. https://doi.org/10.1111/nph.17392 787 Beer, C., Ciais, P., Reichstein, M., Baldocchi, D., Law, B. E., Papale, D., Soussana, J.-F., 788 Ammann, C., Buchmann, N., Frank, D., Gianelle, D., Janssens, I. A., Knohl, A., Köstner, 789 790 B., Moors, E., Roupsard, O., Verbeeck, H., Vesala, T., Williams, C. A., & Wohlfahrt, G. (2009). Temporal and among-site variability of inherent water use efficiency at the 791 ecosystem level. Global Biogeochemical Cycles, 23(2). 792 https://doi.org/10.1029/2008GB003233 793 Beer, C., Reichstein, M., Tomelleri, E., Ciais, P., Jung, M., Carvalhais, N., Rodenbeck, C., 794 Arain, M. A., Baldocchi, D., Bonan, G. B., Bondeau, A., Cescatti, A., Lasslop, G., 795 Lindroth, A., Lomas, M., Luyssaert, S., Margolis, H., Oleson, K. W., Roupsard, O., ... 796 Papale, D. (2010). Terrestrial gross carbon dioxide uptake: Global distribution and 797 798 covariation with climate. Science, 329(5993), 834–838. https://doi.org/10.1126/science.1184984 799 Béland, M., & Baldocchi, D. D. (2021). Vertical structure heterogeneity in broadleaf forests: 800 801 Effects on light interception and canopy photosynthesis. Agricultural and Forest Meteorology, 307, 108525. https://doi.org/10.1016/j.agrformet.2021.108525 802 803 Béland, M., & Kobayashi, H. (2021). Mapping forest leaf area density from multiview terrestrial 804 lidar. Methods in Ecology and Evolution, 12(4), 619–633. https://doi.org/10.1111/2041-805 210X.13550 Belelli, L., Papale, D., & Valentini, R. (2002-2004). FLUXNET2015 RU-Ha1 Hakasia steppe 806 807 [Dataset]. FLUXNET. https://doi.org/10.18140/FLX/1440184

Berbigier, P., Bonnefond, J., Bosc, A., Trichet, P., & Loustau, D. (1996-808 2008). FLUXNET2015 FR-LBr Le Bray [Dataset]. FLUXNET. 809 https://doi.org/10.18140/FLX/1440163 810 Beringer, J., Cunningham, S., Baker, P., Cavagnaro, T., MacNally, R., Thompson, R., & 811 McHugh, I. (2011-2014). FLUXNET2015 AU-Whr Whroo [Dataset]. FLUXNET. 812 https://doi.org/10.18140/FLX/1440206 813 Beringer, J., & Hutley, L. (2007-2013). FLUXNET2015 AU-DaP Daly River Savanna [Dataset]. 814 FLUXNET. https://doi.org/10.18140/FLX/1440123 815 Beringer, J., & Hutley, L. (2008-2014). FLUXNET2015 AU-DaS Daly River Cleared 816 [Dataset]. FLUXNET. https://doi.org/10.18140/FLX/1440122 817 Beringer, J. & Hutley, L. (2008-2014). FLUXNET2015 AU-Dry Dry River 818 [Dataset]. FLUXNET. https://doi.org/10.18140/FLX/1440197 819 Beringer, J., & Hutley, L. (2001-2014). FLUXNET2015 AU-How Howard Springs 820 [Dataset]. FLUXNET. https://doi.org/10.18140/FLX/1440125 821 Beringer, J., & Hutley, L. (2008-2014). FLUXNET2015 AU-Stp Sturt Plains 822 [Dataset]. FLUXNET. https://doi.org/10.18140/FLX/1440204 823 824 Beringer, J., Hutley, L., McGuire, D., Paw U, K. T., & McHugh, I. (2005-2008). FLUXNET2015 AU-Wac Wallaby Creek [Dataset]. FLUXNET. 825 https://doi.org/10.18140/FLX/1440127 826 827 Bernhofer, C., Grünwald, T., Moderow, U., Hehn, M., Eichelmann, U., Prasse, H., & Postel, 828 U. (2004-2014). FLUXNET2015 DE-Gri Grillenburg [Dataset]. FLUXNET. https://doi.org/10.18140/FLX/1440147 829

830	Bernhofer, C., Grünwald, T., Moderow, U., Hehn, M., Eichelmann, U., Prasse, H., & Postel,
831	U. (2008-2014). FLUXNET2015 DE-Obe Oberbärenburg [Dataset]. FLUXNET.
832	https://doi.org/10.18140/FLX/1440151
833	
834	Bernhofer, C., Grünwald, T., Moderow, U., Hehn, M., Eichelmann, U., Prasse, H., & Postel,
835	U. (1996-2014). FLUXNET2015 DE-Tha Tharandt [Dataset]. FLUXNET.
836	https://doi.org/10.18140/FLX/1440152
837	Berninger, F., & Hari, P. (1993). Optimal regulation of gas exchange: Evidence from field data.
838	Annals of Botany, 71(2), 135-140. https://doi.org/10.1006/anbo.1993.1017
839	Berveiller, D., Delpierre, N., Dufrêne, E., Pontailler, J. Y., Vanbostal, L., Janvier, B., Mottet, L.
840	& Cristinacce, K. (2005-2014). FLUXNET2015 FR-Fon Fontainebleau-Barbeau
841	[Dataset]. FLUXNET. https://doi.org/10.18140/FLX/1440161
842	Bonal, D., & Burban, B. (2004-2014). FLUXNET2015 GF-Guy Guyaflux (French Guiana)
843	[Dataset]. FLUXNET. https://doi.org/10.18140/FLX/1440165
844	Bonan, G. B., Williams, M., Fisher, R. A., & Oleson, K. W. (2014). Modeling stomatal
845	conductance in the earth system: Linking leaf water-use efficiency and water transport
846	along the soil-plant-atmosphere continuum. Geoscientific Model Development, 7(5),
847	2193-2222. https://doi.org/10.5194/gmd-7-2193-2014
848	Brodribb, T. J., Holbrook, N. M., Zwieniecki, M. A., & Palma, B. (2005). Leaf hydraulic
849	capacity in ferns, conifers and angiosperms: Impacts on photosynthetic maxima. New
850	Phytologist, 165(3), 839–846. https://doi.org/10.1111/j.1469-8137.2004.01259.x

Brümmer, C., Lucas-Moffat, A., Herbst, M., Kolle, O., & Delorme, J. P. (2001-851 2014). FLUXNET2015 DE-Geb Gebesee [Dataset]. FLUXNET. 852 https://doi.org/10.18140/FLX/1440146 853 Buckley, T. N. (2017). Modeling stomatal conductance. *Plant Physiology*, 174(2), 572–582. 854 https://doi.org/10.1104/pp.16.01772 855 856 Buysse, P., Durand, B., Gueudet, J. C., Mascher, N., Larmanou, E., Cellier, P., & Loubet, B. (2004-2014). FLUXNET2015 FR-Gri Grignon [Dataset]. FLUXNET. 857 https://doi.org/10.18140/FLX/1440162 858 Von Caemmerer, S. (2000). Biochemical models of leaf photosynthesis. Csiro publishing. 859 https://doi.org/10.1071/9780643103405 860 Campbell, G. S. (1974). A simple method for determining unsaturated conductivity from 861 moisture retention data. Soil Science, 117(6), 311-314. https://doi.org/10.1097/00010694-862 197406000-00001 863 Cañete, E., Ortiz, P., Jiménez, M., Poveda, F., Priego, O., Ballesteros, A., & Kowalski, A. (2004-864 2013). FLUXNET2015 ES-LJu Llano de los Juanes [Dataset]. FLUXNET. 865 https://doi.org/10.18140/FLX/1440157 866 867 Cleverly, J., Eamus, D., & Isaac, P. (2010-2014). FLUXNET2015 AU-ASM Alice Springs [Dataset]. FLUXNET. https://doi.org/10.18140/FLX/1440194 868 869 Cleverly, J., Eamus, D., Isaac, P. (2012-2014). FLUXNET2015 AU-TTE Ti Tree East [Dataset]. 870 FLUXNET. https://doi.org/10.18140/FLX/1440205 Cowan, I. R. (1982). Regulation of Water Use in Relation to Carbon Gain in Higher Plants. In: 871 O. L. Lange, P. S. Nobel, C. B. Osmond, & H. Ziegler (Eds.), Physiological Plant 872

873	Ecology II: Water Relations and Carbon Assimilation, pp. 589-613. Springer.
874	https://doi.org/10.1007/978-3-642-68150-9_18
875	Cowan, I. R., & Farquhar, G. D. (1977). Stomatal function in relation to leaf metabolism and
876	environment. Symposia of the Society for Experimental Biology, 31, 471–505.
877	Cremonese, E., Galvagno, M., di Cella, U., & Migliavacca, M. (2008-2014). FLUXNET2015 IT
878	Tor Torgnon [Dataset]. FLUXNET. https://doi.org/10.18140/FLX/1440237
879	Dolman, H., van der Molen, M., Parmentier, F. J., Marchesini, L., Dean, J., van Huissteden,
880	K., & Maximov, T. (2003-2014). FLUXNET2015 RU-Cok Chokurdakh
881	[Dataset]. FLUXNET. https://doi.org/10.18140/FLX/1440182
882	Dong, G. (2007-2010). FLUXNET2015 CN-Cng Changling [Dataset]. FLUXNET.
883	https://doi.org/10.18140/FLX/1440209
884	Farquhar, G. D. (1978). Feedforward responses of stomata to humidity. Australian Journal of
885	Plant Physiology, 5(6), 787–800. https://doi.org/10.1071/PP9780787
886	Farquhar, G. D., von Caemmerer, S., & Berry, J. A. (1980a). A biochemical model of
887	photosynthetic CO <sub>2</sub> assimilation in leaves of C <sub>3</sub> species. <i>Planta</i> , 149(1), 78–90.
888	https://doi.org/10.1007/BF00386231
889	Farquhar, G. D., Schulze, E. D., & Kuppers, M. (1980b). Responses to humidity by stomata of
890	Nicotiana glauca L. and Corylus avellana L. are consistent with the optimization of
891	carbon dioxide uptake with respect to water loss. Australian Journal of Plant Physiology,
892	7(3), 315–327. https://doi.org/10.1071/PP9800315
893	Feldman, A. F., Short Gianotti, D. J., Trigo, I. F., Salvucci, G. D., & Entekhabi, D. (2019).
894	Satellite-based assessment of land surface energy partitioning-soil moisture relationships

895	and effects of confounding variables. Water Resources Research, 55(12), 10657–10677.
896	https://doi.org/10.1029/2019WR025874
897	Feng, X., Lu, Y., Jiang, M., Katul, G., Manzoni, S., Mrad, A., & Vico, G. (2022). Instantaneous
898	stomatal optimization results in suboptimal carbon gain due to legacy effects. Plant, Cell
899	& Environment, 45(11), 3189-3204. https://doi.org/10.1111/pce.14427
900	Ficklin, D. L., & Novick, K. A. (2017). Historic and projected changes in vapor pressure deficit
901	suggest a continental-scale drying of the United States atmosphere. Journal of
902	Geophysical Research: Atmospheres, 122(4), 2061–2079.
903	https://doi.org/10.1002/2016JD025855
904	Finnigan, J. J., & Raupach, M. R. (1987). Transfer processes in plant canopies in relation to
905	stomatal characteristics. Stomatal Function, 385-429.
906	https://www.cabdirect.org/cabdirect/abstract/19880712530
907	Fites, J. A., & Teskey, R. O. (1988). CO <sub>2</sub> and water vapor exchange of <i>Pinustaeda</i> in relation to
908	stomatal behavior: Test of an optimization hypothesis. Canadian Journal of Forest
909	Research, 18(2), 150–157. https://doi.org/10.1139/x88-024
910	FLUXNET2015 CA-NS1 UCI-1850 burn site [Dataset]. (2001-2005).
911	FLUXNET. https://doi.org/10.18140/FLX/1440036
912	FLUXNET2015 CA-NS2 UCI-1930 burn site [Dataset]. (2001-2005).
913	FLUXNET. https://doi.org/10.18140/FLX/1440037
914	FLUXNET2015 CA-NS3 UCI-1964 burn site [Dataset]. (2001-2005). FLUXNET.
915	https://doi.org/10.18140/FLX/1440038
916	FLUXNET2015 CA-NS4 UCI-1964 burn site wet [Dataset]. (2002-2005). FLUXNET.
917	https://doi.org/10.18140/FLX/1440039

918	FLUXNET2015 CA-NS5 UCI-1981 burn site [Dataset]. (2001-2005). FLUXNET.
919	https://doi.org/10.18140/FLX/1440040
920	FLUXNET2015 CA-NS6 UCI-1989 burn site [Dataset]. (2001-2005). FLUXNET.
921	https://doi.org/10.18140/FLX/1440041
922	FLUXNET2015 CA-NS7 UCI-1998 burn site [Dataset]. (2002-2005). FLUXNET.
923	https://doi.org/10.18140/FLX/1440042
924	FLUXNET2015 CA-Oas Saskatchewan - Western Boreal, Mature Aspen [Dataset]. (1996-2010)
925	FLUXNET. https://doi.org/10.18140/FLX/1440043
926	FLUXNET2015 CA-Obs Saskatchewan - Western Boreal, Mature Black Spruce [Dataset].
927	(1997-2010). FLUXNET. https://doi.org/10.18140/FLX/1440044
928	FLUXNET2015 CA-Qfo Quebec - Eastern Boreal, Mature Black Spruce [Dataset]. (2003-2010)
929	FLUXNET. https://doi.org/10.18140/FLX/1440045
930	FLUXNET2015 CA-SF1 Saskatchewan - Western Boreal, forest burned in 1977 [Dataset].
931	(2003-2006). FLUXNET. https://doi.org/10.18140/FLX/1440046
932	FLUXNET2015 CA-SF2 Saskatchewan - Western Boreal, forest burned in 1989 [Dataset].
933	(2001-2005). FLUXNET. https://doi.org/10.18140/FLX/1440047
934	FLUXNET2015 CA-SF3 Saskatchewan - Western Boreal, forest burned in 1998 [Dataset].
935	(2001-2006). FLUXNET. https://doi.org/10.18140/FLX/1440048
936	FLUXNET2015 CA-TP1 Ontario - Turkey Point 2002 Plantation White Pine [Dataset]. (2002-
937	2014). FLUXNET. https://doi.org/10.18140/FLX/1440050
938	FLUXNET2015 CA-TP2 Ontario - Turkey Point 1989 Plantation White Pine [Dataset]. (2002-
939	2007). FLUXNET. https://doi.org/10.18140/FLX/1440051

940	FLUXNET2015 CA-TP3 Ontario - Turkey Point 1974 Plantation White Pine [Dataset]. (2002-
941	2014). FLUXNET. https://doi.org/10.18140/FLX/1440052
942	FLUXNET2015 CA-TP4 Ontario - Turkey Point 1939 Plantation White Pine [Dataset]. (2002-
943	2014). FLUXNET. https://doi.org/10.18140/FLX/1440053
944	FLUXNET2015 CA-TPD Ontario - Turkey Point Mature Deciduous [Dataset]. (2012-
945	2014). FLUXNET. https://doi.org/10.18140/FLX/1440112
946	FLUXNET2015 US-AR1 ARM USDA UNL OSU Woodward Switchgrass 1 [Dataset]. (2009-
947	2012). FLUXNET. https://doi.org/10.18140/FLX/1440103
948	FLUXNET2015 US-AR2 ARM USDA UNL OSU Woodward Switchgrass 2 [Dataset]. (2009-
949	2012). FLUXNET. https://doi.org/10.18140/FLX/1440104
950	FLUXNET2015 US-ARM ARM Southern Great Plains site- Lamont [Dataset]. (2003-2012).
951	FLUXNET. https://doi.org/10.18140/FLX/1440066
952	FLUXNET2015 US-Blo Blodgett Forest [Dataset]. (1997-2007).
953	FLUXNET. https://doi.org/10.18140/FLX/1440068
954	FLUXNET2015 US-CRT Curtice Walter-Berger cropland [Dataset]. (2011-2013). FLUXNET.
955	https://doi.org/10.18140/FLX/1440117
956	FLUXNET2015 US-Cop Corral Pocket [Dataset]. (2001-2007).
957	FLUXNET. https://doi.org/10.18140/FLX/1440100
958	FLUXNET2015 US-GLE GLEES [Dataset]. (2004-2014).
959	FLUXNET. https://doi.org/10.18140/FLX/1440069
960	FLUXNET2015 US-Ha1 Harvard Forest EMS Tower (HFR1) [Dataset]. (1991-2012).
961	FLUXNET. https://doi.org/10.18140/FLX/1440071

962	FLUXNET2015 US-IB2 Fermi National Accelerator Laboratory- Batavia (Prairie site)
963	[Dataset]. (2004-2011). FLUXNET. https://doi.org/10.18140/FLX/1440072
964	FLUXNET2015 US-KS2 Kennedy Space Center (scrub oak) [Dataset]. (2003-2006).
965	FLUXNET. https://doi.org/10.18140/FLX/1440075
966	FLUXNET2015 US-Me2 Metolius mature ponderosa pine [Dataset]. (2002-2014). FLUXNET
967	https://doi.org/10.18140/FLX/1440079
968	FLUXNET2015 US-Me3 Metolius-second young aged pine [Dataset]. (2004-2009).
969	FLUXNET. https://doi.org/10.18140/FLX/1440080
970	FLUXNET2015 US-Me4 Metolius-old aged ponderosa pine [Dataset]. (1996-2000).
971	FLUXNET. https://doi.org/10.18140/FLX/1440081
972	FLUXNET2015 US-Me5 Metolius-first young aged pine [Dataset]. (2000-
973	2002). FLUXNET. https://doi.org/10.18140/FLX/1440082
974	FLUXNET2015 US-Me6 Metolius Young Pine Burn [Dataset]. (2010-2014).
975	FLUXNET. https://doi.org/10.18140/FLX/1440099
976	FLUXNET2015 US-MMS Morgan Monroe State Forest [Dataset]. (1999-2014).
977	FLUXNET. https://doi.org/10.18140/FLX/1440083
978	FLUXNET2015 US-Ne3 Mead - rainfed maize-soybean rotation site [Dataset]. (2001-2013).
979	FLUXNET. https://doi.org/10.18140/FLX/1440086
980	FLUXNET2015 US-NR1 Niwot Ridge Forest (LTER NWT1) [Dataset]. (1998-2014).
981	FLUXNET. https://doi.org/10.18140/FLX/1440087
982	FLUXNET2015 US-Oho Oak Openings [Dataset]. (2004-2013).
983	FLUXNET. https://doi.org/10.18140/FLX/1440088

FLUXNET2015 US-SRC Santa Rita Creosote [Dataset]. (2008-2014). 984 FLUXNET. https://doi.org/10.18140/FLX/1440098 985 986 FLUXNET2015 US-SRG Santa Rita Grassland [Dataset]. (2008-2014). FLUXNET. https://doi.org/10.18140/FLX/1440114 987 FLUXNET2015 US-SRM Santa Rita Mesquite [Dataset]. (2004-2014). 988 FLUXNET. https://doi.org/10.18140/FLX/1440090 989 FLUXNET2015 US-Ton Tonzi Ranch [Dataset]. (2001-2014). 990 FLUXNET. https://doi.org/10.18140/FLX/1440092 991 FLUXNET2015 US-Twt Twitchell Island [Dataset]. (2009-2014). 992 FLUXNET. https://doi.org/10.18140/FLX/1440106 993 FLUXNET2015 US-UMB Univ. of Mich. Biological Station [Dataset]. (2000-2014). 994 FLUXNET. https://doi.org/10.18140/FLX/1440093 995 FLUXNET2015 US-Var Vaira Ranch- Ione [Dataset]. (2000-2014). 996 997 FLUXNET. https://doi.org/10.18140/FLX/1440094 FLUXNET2015 US-Whs Walnut Gulch Lucky Hills Shrub [Dataset]. (2007-2014). 998 FLUXNET. https://doi.org/10.18140/FLX/1440097 999 1000 FLUXNET2015 US-Wi4 Mature red pine (MRP) [Dataset]. (2002-2005). FLUXNET. https://doi.org/10.18140/FLX/1440058 1001 1002 FLUXNET2015 US-Wkg Walnut Gulch Kendall Grasslands [Dataset]. (2004-2014). 1003 FLUXNET. https://doi.org/10.18140/FLX/1440096 Franks, P. J., Bonan, G. B., Berry, J. A., Lombardozzi, D. L., Holbrook, N. M., Herold, N., & 1004 Oleson, K. W. (2018). Comparing optimal and empirical stomatal conductance models 1005

1006	for application in Earth system models. <i>Global Change Biology</i> , 24(12), 5708–5723.
1007	https://doi.org/10.1111/gcb.14445
1008	van Genuchten, M. Th. (1980). A closed-form equation for predicting the hydraulic conductivity
1009	of unsaturated soils. Soil Science Society of America Journal, 44(5), 892-898.
1010	https://doi.org/10.2136/sssaj1980.03615995004400050002x
1011	Gianelle, D., Cavagna, M., Zampedri, R., & Marcolla, B. (2003-2013). FLUXNET2015 IT-
1012	MBo Monte Bondone [Dataset]. FLUXNET. https://doi.org/10.18140/FLX/1440170
1013	Gianelle, D., Zampedri, R., Cavagna, M., & Sottocornola, M. (2003-2014). FLUXNET2015 IT-
1014	Lav Lavarone [Dataset]. FLUXNET. https://doi.org/10.18140/FLX/1440169
1015	Green, J. K., Seneviratne, S. I., Berg, A. M., Findell, K. L., Hagemann, S., Lawrence, D. M., &
1016	Gentine, P. (2019). Large influence of soil moisture on long-term terrestrial carbon
1017	uptake. Nature, 565(7740), 476–479. https://doi.org/10.1038/s41586-018-0848-x
1018	Grieu, P., Guehl, J. M., & Aussenac, G. (1988). The effects of soil and atmospheric drought on
1019	photosynthesis and stomatal control of gas exchange in three coniferous species.
1020	Physiologia Plantarum, 73(1), 97–104. https://doi.org/10.1111/j.1399-
1021	3054.1988.tb09199.x
1022	Grossiord, C., Buckley, T. N., Cernusak, L. A., Novick, K. A., Poulter, B., Siegwolf, R. T. W.,
1023	Sperry, J. S., & McDowell, N. G. (2020). Plant responses to rising vapor pressure deficit
1024	New Phytologist, 226(6), 1550–1566. https://doi.org/10.1111/nph.16485
1025	Gruening, C., Goded, I., Cescatti, A., Manca, G., & Seufert, G. (1999-
1026	2012). FLUXNET2015 IT-SRo San Rossore [Dataset]. FLUXNET.
1027	https://doi.org/10.18140/FLX/1440176

Hall, A. E., & Schulze, E.-D. (1980). Stomatal response to environment and a possible 1028 interrelation between stomatal effects on transpiration and CO<sub>2</sub> assimilation. *Plant, Cell* 1029 & Environment, 3(6), 467–474. https://doi.org/10.1111/1365-3040.ep11587040 1030 Hari, P., Mäkelä, A., & Pohja, T. (2000). Surprising implications of the optimality hypothesis of 1031 stomatal regulation gain support in a field test. Functional Plant Biology, 27(1), 77–80. 1032 1033 https://doi.org/10.1071/pp99050 Hörtnagl, L., Eugster, W., Merbold, L., Buchmann, N., Gharun, M., Etzold, S., Haesler, R., 1034 Haeni, M., Pluess, P., Meier, P., Käslin, F., & Baur, T. (1997-1035 2014). FLUXNET2015 CH-Dav Davos [Dataset]. 1036 FLUXNET. https://doi.org/10.18140/FLX/1440132 1037 Hörtnagl, L., Feigenwinter, I., Fuchs, K., Merbold, L., Buchmann, N., 1038 Eugster, W., Zeeman, M., Baur, T., Pluess, P., Käslin, F., Meier, P., & Koller, P. (2005-1039 2014). FLUXNET2015 CH-Cha Chamau [Dataset]. FLUXNET. 1040 1041 https://doi.org/10.18140/FLX/1440131 Hörtnagl, L., Feigenwinter, I., Fuchs, K., Merbold, L., Buchmann, N., Eugster, W., Zeeman, M., 1042 Baur, T., Pluess, P., Käslin, F., Meier, P., & Koller, P. (2005-2014). FLUXNET2015 CH-1043 1044 Fru Früebüel [Dataset]. FLUXNET. https://doi.org/10.18140/FLX/1440133 Ibrom, A., & Pilegaard, K. (1996-2014). FLUXNET2015 DK-Sor Soroe [Dataset]. FLUXNET. 1045 1046 https://doi.org/10.18140/FLX/1440155 1047 Jones, H. G. (2014). Plants and Microclimate: A Quantitative Approach to Environmental Plant Physiology. 3rd ed. Cambridge University Press. 1048 Katul, G. G., Palmroth, S., & Oren, R. (2009). Leaf stomatal responses to vapour pressure deficit 1049 1050 under current and CO<sub>2</sub>-enriched atmosphere explained by the economics of gas exchange.

1051	Plant, Cell & Environment, 32(8), 968–979. https://doi.org/10.1111/j.1365-
1052	3040.2009.01977.x
1053	Katul, G., Manzoni, S., Palmroth, S., & Oren, R. (2010). A stomatal optimization theory to
1054	describe the effects of atmospheric CO <sub>2</sub> on leaf photosynthesis and transpiration. Annals
1055	of Botany, 105(3), 431-442. https://doi.org/10.1093/aob/mcp292
1056	Kelliher, F. M., Leuning, R., Raupach, M. R., & Schulze, ED. (1995). Maximum conductances
1057	for evaporation from global vegetation types. Agricultural and Forest Meteorology,
1058	73(1), 1–16. https://doi.org/10.1016/0168-1923(94)02178-M
1059	Kennedy, D., Swenson, S., Oleson, K. W., Lawrence, D.M., Fisher, R., Lola da Costa, A. C., &
1060	Gentine, P. (2019). Implementing plant hydraulics in the Community Land Model,
1061	version 5. Journal of Advances in Modeling Earth Systems, 11(2), 485-513.
1062	https://doi.org/10.1029/2018MS001500
1063	Knauer, J., Werner, C., & Zaehle, S. (2015). Evaluating stomatal models and their atmospheric
1064	drought response in a land surface scheme: A multibiome analysis. Journal of
1065	Geophysical Research: Biogeosciences, 120(10), 1894–1911.
1066	https://doi.org/10.1002/2015JG003114
1067	Knauer, J., Zaehle, S., Medlyn, B. E., Reichstein, M., Williams, C. A., Migliavacca, M., De
1068	Kauwe, M. G., Werner, C., Keitel, C., Kolari, P., Limousin, JM., & Linderson, ML.
1069	(2018). Towards physiologically meaningful water-use efficiency estimates from eddy
1070	covariance data. Global Change Biology, 24(2), 694-710.
1071	https://doi.org/10.1111/gcb.13893

1072	Knohl, A., Tiedemann, F., Kolle, O., Schulze, E. D., Anthoni, P., Kutsch, W., Herbst, M., &
1073	Siebicke, L. (2002-2012). FLUXNET2015 DE-Lnf Leinefelde [Dataset]. FLUXNET.
1074	https://doi.org/10.18140/FLX/1440150
1075	Knohl, A., Tiedemann, F., Kolle, O., Schulze, E. D., Kutsch, W., Herbst, M., & Siebicke,
1076	L. (2000-2012). FLUXNET2015 DE-Hai Hainich [Dataset]. FLUXNET.
1077	https://doi.org/10.18140/FLX/1440148
1078	Kutsch, W., Merbold, L., & Kolle, O. (2000-2009). FLUXNET2015 ZM-Mon Mongu [Dataset].
1079	FLUXNET. https://doi.org/10.18140/FLX/1440189
1080	Lanning, M., Wang, L., & Novick, K. A. (2020). The importance of cuticular permeance in
1081	assessing plant water-use strategies. Tree Physiology, 40(4), 425-432.
1082	https://doi.org/10.1093/treephys/tpaa020
1083	Lasslop, G., Reichstein, M., Papale, D., Richardson, A. D., Arneth, A., Barr, A., Stoy, P., &
1084	Wohlfahrt, G. (2010). Separation of net ecosystem exchange into assimilation and
1085	respiration using a light response curve approach: critical issues and global evaluation.
1086	Global Change Biology, 16(1), 187–208. https://doi.org/10.1111/j.1365-
1087	2486.2009.02041.x
1088	Lawlor, D. W., & Tezara, W. (2009). Causes of decreased photosynthetic rate and metabolic
1089	capacity in water-deficient leaf cells: A critical evaluation of mechanisms and integration
1090	of processes. Annals of Botany, 103(4), 561-579. https://doi.org/10.1093/aob/mcn244
1091	Leuning, R. (1995). A critical appraisal of a combined stomatal-photosynthesis model for C <sub>3</sub>
1092	plants. Plant, Cell & Environment., 18(4), 339–355. https://doi.org/10.1111/j.1365-
1093	3040.1995.tb00370.x

Lin, C., Gentine, P., Huang, Y., Guan, K., Kimm, H., & Zhou, S. (2018). Diel ecosystem 1094 conductance response to vapor pressure deficit is suboptimal and independent of soil 1095 moisture. Agricultural and Forest Meteorology, 250–251, 24–34. 1096 https://doi.org/10.1016/j.agrformet.2017.12.078 1097 Lin, Y.-S., Medlyn, B. E., Duursma, R. A., Prentice, I. C., Wang, H., Baig, S., Eamus, D., de 1098 Dios, V. R., Mitchell, P., Ellsworth, D. S., de Beeck, M. O., Wallin, G., Uddling, J., 1099 Tarvainen, L., Linderson, M.-L., Cernusak, L. A., Nippert, J. B., Ocheltree, T. W., 1100 Tissue, D. T., ... Wingate, L. (2015). Optimal stomatal behaviour around the world. 1101 *Nature Climate Change*, 5(5), 459–464. https://doi.org/10.1038/nclimate2550 1102 Lindauer, M., Steinbrecher, R., Wolpert, B., Mauder, M., & Schmid, H. (2009-1103 2013). FLUXNET2015 DE-Lkb Lackenberg [Dataset]. FLUXNET. 1104 https://doi.org/10.18140/FLX/1440214 1105 Lohila, A., Aurela, M., Tuovinen, J. P., Hatakka, J., & Laurila, T. (2000-1106 1107 2003). FLUXNET2015 FI-Jok Jokioinen [Dataset]. FLUXNET. https://doi.org/10.18140/FLX/1440159 1108 Lohila, A., Korkiakoski, M., Tuovinen, J. P., Hatakka, J., Aurela, M., Rainne, J., Mäkelä, T., & 1109 1110 Laurila, T. (2009-2012). FLUXNET2015 FI-Let Lettosuo [Dataset]. FLUXNET. https://doi.org/10.18140/FLX/1440227 1111 1112 Loveland, T. R., & Belward, A. S. (1997). The International Geosphere Biosphere Programme 1113 Data and Information System global land cover data set (DISCover). Acta Astronautica, 41(4-10), 681–689. https://doi.org/10.1016/S0094-5765(98)00050-2 1114

Lu, Y., Duursma, R. A., Farrior, C. E., Medlyn, B. E., & Feng, X. (2020). Optimal stomatal 1115 drought response shaped by competition for water and hydraulic risk can explain plant 1116 trait covariation. New Phytologist, 225(3), 1206–1217. https://doi.org/10.1111/nph.16207 1117 Lu, Y. J., Duursma, R. A., & Medlyn, B. E. (2016). Optimal stomatal behaviour under stochastic 1118 rainfall. Journal of Theoretical Biology, 394, 160–171. 1119 https://doi.org/10.1016/j.jtbi.2016.01.003 1120 Lund, M., Jackowicz-Korczyński, M., & Abermann, J. (2000-2014). FLUXNET2015 GL-1121 ZaH Zackenberg Heath [Dataset]. FLUXNET. https://doi.org/10.18140/FLX/1440224 1122 Macfarlane, C., Lambert, P., Byrne, J., Johnstone, C., & Smart, N. (2011-1123 2014). FLUXNET2015 AU-Gin Gingin [Dataset]. 1124 FLUXNET. https://doi.org/10.18140/FLX/1440199 1125 Magliulo, V., Tommasi, P., Famulari, D., Gasbarra, D., Vitale, L., Manco, A., Esposito, A., 1126 Tosca, M., & di Matteo, F. (2004-2014). FLUXNET2015 IT-BCi Borgo Cioffi 1127 [Dataset]. FLUXNET. https://doi.org/10.18140/FLX/1440166 1128 Mäkelä, A., Berninger, F., & Hari, P. (1996). Optimal control of gas exchange during drought: 1129 Theoretical analysis. *Annals of Botany*, 77(5), 461–467. 1130 1131 https://www.jstor.org/stable/42764687 Mammarella, I., Keronen, P., Kolari, P., Launiainen, S., Pumpanen, J., Rannik, Ü., Siivola, 1132 1133 E., Levula, J., Pohja, T., & Vesala, T. (1996-2014). FLUXNET2015 FI-Hyy Hyytiala 1134 [Dataset]. FLUXNET. https://doi.org/10.18140/FLX/1440158 Manca, G., & Goded, I. (2002-2004). FLUXNET2015 IT-PT1 Parco Ticino forest [Dataset]. 1135 FLUXNET. https://doi.org/10.18140/FLX/1440172 1136

Manzoni, S., Vico, G., Katul, G., Fay, P. A., Polley, W., Palmroth, S., & Porporato, A. (2011). 1137 Optimizing stomatal conductance for maximum carbon gain under water stress: A meta-1138 analysis across plant functional types and climates. Functional Ecology, 25(3), 456–467. 1139 https://doi.org/10.1111/j.1365-2435.2010.01822.x 1140 Manzoni, S., Vico, G., Palmroth, S., Porporato, A., & Katul, G. (2013). Optimization of stomatal 1141 1142 conductance for maximum carbon gain under dynamic soil moisture. Advances in Water Resources, 62, 90–105. https://doi.org/10.1016/j.advwatres.2013.09.020 1143 Marshall, B. & Biscoe, P. V. (1980). A model for C<sub>3</sub> leaves describing the dependence of net 1144 photosynthesis on irradiance, Journal of Experimental Botany, 31(1), 29– 1145 39. https://doi.org/10.1093/jxb/31.1.29 1146 Martinez-Vilalta, J., Poyatos, R., Aguade, D., Retana, J., & Mencuccini, M. (2014). A new look 1147 at water transport regulation in plants. New Phytologist, 204(1), 105–115. 1148 https://doi.org/10.1111/nph.12912 1149 Matteucci, G. (1996-2014). FLUXNET2015 IT-Col Collelongo [Dataset]. 1150 FLUXNET. https://doi.org/10.18140/FLX/1440167 1151 Medlyn, B. E., De Kauwe, M. G., Lin, Y.-S., Knauer, J., Duursma, R. A., Williams, C. A., 1152 1153 Arneth, A., Clement, R., Isaac, P., Limousin, J.-M., Linderson, M.-L., Meir, P., Martin-StPaul, N., & Wingate, L. (2017). How do leaf and ecosystem measures of water-use 1154 efficiency compare? New Phytologist, 216(3), 758-770. 1155 1156 https://doi.org/10.1111/nph.14626. Medlyn, B. E., Duursma, R. A., Eamus, D., Ellsworth, D. S., Colin Prentice, I., Barton, C. V. M., 1157 Crous, K. Y., de Angelis, P., Freeman, M., & Wingate, L. (2012). Reconciling the 1158

optimal and empirical approaches to modelling stomatal conductance. Global Change 1159 Biology, 18(11), 3476–3476. https://doi.org/10.1111/j.1365-2486.2012.02790.x 1160 Meyer, W., Cale, P., Koerber, G., Ewenz, C., & Sun, Q. (2010-2014). FLUXNET2015 AU-1161 Cpr Calperum [Dataset]. FLUXNET. https://doi.org/10.18140/FLX/1440195 1162 Michaelis, L. & Menten, M. L. (1913). Die kinetik der invertinwirkung. Biochem. z, 49(333-1163 369), 352. 1164 Montagnani, L., & Minerbi, S. (1998-2013). FLUXNET2015 IT-Ren Renon 1165 [Dataset]. FLUXNET. https://doi.org/10.18140/FLX/1440173 1166 Monteith, J. L. (1965). Evaporation and environment. Symposia of the Society for Experimental 1167 Biology, 19, 205–234. 1168 Moors, E., & Elbers, J. (1996-2014). FLUXNET2015 NL-Loo Loobos [Dataset]. FLUXNET. 1169 https://doi.org/10.18140/FLX/1440178 1170 Nouvellon, Y. (2006-2009). FLUXNET2015 CG-Tch Tchizalamou [Dataset]. 1171 1172 FLUXNET. https://doi.org/10.18140/FLX/1440142 Novick, K. A., & Barnes, M. L. (2023). A practical exploration of land cover impacts on surface 1173 and air temperature when they are most consequential. Environmental Research: Climate, 1174 1175 2(2), 025007. https://doi.org/10.1088/2752-5295/accdf9 Novick, K. A., Ficklin, D. L., Baldocchi, D., Davis, K. J., Ghezzehei, T. A., Konings, A. G., 1176 1177 MacBean, N., Raoult, N., Scott, R. L., Shi, Y., Sulman, B. N., & Wood, J. D. (2022). 1178 Confronting the water potential information gap. *Nature Geoscience*, 15, 158–164. 1179 https://doi.org/10.1038/s41561-022-00909-2 Novick, K. A., Ficklin, D. L., Stoy, P. C., Williams, C. A., Bohrer, G., Oishi, A. C., Papuga, S. 1180 1181 A., Blanken, P. D., Noormets, A., Sulman, B. N., Scott, R. L., Wang, L., & Phillips, R. P.

1182	(2016a). The increasing importance of atmospheric demand for ecosystem water and
1183	carbon fluxes. Nature Climate Change, 6, 1023–1027.
1184	https://doi.org/10.1038/nclimate3114
1185	Novick, K. A., Konings, A. G., & Gentine, P. (2019). Beyond soil water potential: An expanded
1186	view on isohydricity including land-atmosphere interactions and phenology. Plant, Cell
1187	& Environment, 42(6), 1802–1815. https://doi.org/10.1111/pce.13517
1188	Novick, K. A., Miniat, C. F., & Vose, J. M. (2016b). Drought limitations to leaf-level gas
1189	exchange: Results from a model linking stomatal optimization and cohesion-tension
1190	theory. Plant, Cell & Environment, 39(3), 583-596. https://doi.org/10.1111/pce.12657
1191	Ourcival, J. M., Piquemal, K., Joffre, R., & Jean-Marc, L. (2000-2014). FLUXNET2015 FR-
1192	Pue Puechabon [Dataset]. FLUXNET. https://doi.org/10.18140/FLX/1440164
1193	Papale, D., Arriga, N., Belelli, L., Consalvo, C., Dore, S., Manca, G., Mazzenga, F.,
1194	Sabbatini, S., Stefani, P., Tirone, G., Valentini, R., Boschi, A., & Tomassucci, M. (2002-
1195	2012). FLUXNET2015 IT-Ro2 Roccarespampani 2 [Dataset]. FLUXNET.
1196	https://doi.org/10.18140/FLX/1440175
1197	Pastorello, G., Trotta, C., Canfora, E., Chu, H., Christianson, D., Cheah, YW., Poindexter, C.,
1198	Chen, J., Elbashandy, A., Humphrey, M., Isaac, P., Polidori, D., Reichstein, M., Ribeca,
1199	A., van Ingen, C., Vuichard, N., Zhang, L., Amiro, B., Ammann, C., Papale, D.
1200	(2020). The FLUXNET2015 dataset and the ONEFlux processing pipeline for eddy
1201	covariance data. Scientific Data, 7, 225. https://doi.org/10.1038/s41597-020-0534-3
1202	Paw U, K. T., & Meyers, T. P. (1989). Investigations with a higher-order canopy turbulence
1203	model into mean source-sink levels and bulk canopy resistances. Agricultural and Forest
1204	Meteorology, 47(2), 259-271. https://doi.org/10.1016/0168-1923(89)90099-3

1205	Pendall, E., Griebel, A., Metzen, D., & Barton, C. (2012-2014). FLUXNET2015 AU-
1206	Cum Cumberland Plain [Dataset]. FLUXNET. https://doi.org/10.18140/FLX/1440196
1207	Pilegaard, K., & Ibrom, A. (2005-2008). FLUXNET2015 DK-Eng Enghave
1208	[Dataset]. FLUXNET. https://doi.org/10.18140/FLX/1440153
1209	Posse, G., Lewczuk, N., Richter, K., & Cristiano, P. (2009-2012). FLUXNET2015 AR-Vir
1210	Virasoro [Dataset]. FLUXNET. https://doi.org/10.18140/FLX/1440192
1211	Poveda, F., Ballesteros, A., Cañete, E., Ortiz, P., Jiménez, M., Priego, O., & Kowalski, A. (2007-
1212	2012). FLUXNET2015 ES-Amo Amoladeras [Dataset]. FLUXNET.
1213	https://doi.org/10.18140/FLX/1440156
1214	Reverter, B., Perez-Cañete, E., & Kowalski, A. (2007-2009). FLUXNET2015 ES-LgS Laguna
1215	Seca [Dataset]. FLUXNET. https://doi.org/10.18140/FLX/1440225
1216	Sabbatini, S., Arriga, N., Matteucci, G., Papale, D., Tomassucci, M., & Boschi, A. (2011-
1217	2014). FLUXNET2015 IT-CA3 Castel d'Asso3 [Dataset]. FLUXNET.
1218	https://doi.org/10.18140/FLX/1440232
1219	Sabbatini, S., Arriga, N., Papale, D., Tomassucci, M., & Boschi, A. (2011-
1220	2014). FLUXNET2015 IT-CA1 Castel d'Asso1 [Dataset]. FLUXNET.
1221	https://doi.org/10.18140/FLX/1440230
1222	Sabot, M. E. B., De Kauwe, M. G., Pitman, A. J., Medlyn, B. E., Ellsworth, D. S., Martin-StPaul
1223	N. K., Wu, J., Choat, B., Limousin, JM., Mitchell, P. J., Rogers, A., & Serbin, S. P.
1224	(2022). One stomatal model to rule them all? Toward improved representation of carbon
1225	and water exchange in global models. Journal of Advances in Modeling Earth Systems,
1226	14(4), e2021MS002761. https://doi.org/10.1029/2021MS002761

1227	Schneider, K., & Schmidt, M. (2007-2010). FLUXNET2015 DE-Seh Selhausen
1228	[Dataset]. FLUXNET. https://doi.org/10.18140/FLX/1440217
1229	Schroder, I., Zegelin, S., Palu, T., & Feitz, A. (2011-2013). FLUXNET2015 AU-Emr Emerald
1230	[Dataset]. FLUXNET. https://doi.org/10.18140/FLX/1440198
1231	Sigut, L., Havrankova, K., Jocher, G., Pavelka, M., Janouš, D., Stanik, K., Trusina, J., & Czerny,
1232	R. (2004-2014). FLUXNET2015 CZ-BK1 Bily Kriz forest [Dataset].
1233	FLUXNET. https://doi.org/10.18140/FLX/1440143
1234	Sigut, L., Havrankova, K., Jocher, G., Pavelka, M., Janouš, D., Stanik, K., Trusina, J., & Czerny,
1235	R. (2004-2012). FLUXNET2015 CZ-BK2 Bily Kriz grassland [Dataset]. FLUXNET.
1236	https://doi.org/10.18140/FLX/1440144
1237	Spano, D., Duce, P., Marras, S., Sirca, C., Mereu, S., Arca, A., Zara, P., Ventura, A., & Sanna,
1238	L. (2004-2014). FLUXNET2015 IT-Noe Arca di Noe - Le Prigionette
1239	[Dataset]. FLUXNET. https://doi.org/10.18140/FLX/1440171
1240	Sperry, J. S., Venturas, M. D., Anderegg, W. R. L., Mencuccini, M., Mackay, D. S., Wang, Y., &
1241	Love, D. M. (2017). Predicting stomatal responses to the environment from the
1242	optimization of photosynthetic gain and hydraulic cost. Plant, Cell & Environment,
1243	40(6), 816–830. https://doi.org/10.1111/pce.12852
1244	Stocker, B. D., Zscheischler, J., Keenan, T. F., Prentice, I. C., Peñuelas, J., & Seneviratne, S. I.
1245	(2018). Quantifying soil moisture impacts on light use efficiency across biomes. New
1246	Phytologist, 218(4), 1430-1449. https://doi.org/10.1111/nph.15123
1247	Thornley, J. H. (1976). Mathematical Models in Plant Physiology. Academic Press (Inc.)
1248	London, Ltd.

United Nations Environment Programme (1992). World Atlas of Desertification. 1249 https://wedocs.unep.org/20.500.11822/42137. 1250 Valentini, R., Arriga, N., Belelli, L., Dore, S., Manca, G., Mazzenga, F., 1251 Pegoraro, E., Sabbatini, S., Stefani, P., Tirone, G., Vitale, D., Papale, D., Boschi, A., & 1252 Tomassucci, M. (2000-2008). FLUXNET2015 IT-Ro1 Roccarespampani 1 1253 1254 [Dataset]. FLUXNET. https://doi.org/10.18140/FLX/1440174 Valentini, R., Dore, S., Mazzenga, F., Sabbatini, S., Stefani, P., Tirone, G., & Papale, D. (1997-1255 2009). FLUXNET2015 IT-Cpz Castelporziano [Dataset]. FLUXNET. 1256 https://doi.org/10.18140/FLX/1440168 1257 Varlagin, A., Kurbatova, J., & Vygodskaya, N. (1998-2014). FLUXNET2015 RU-1258 Fyo Fyodorovskoye [Dataset]. FLUXNET. https://doi.org/10.18140/FLX/1440183 1259 Wang, Y., Sperry, J. S., Anderegg, W. R. L., Venturas, M. D., & Trugman, A. T. (2020). A 1260 theoretical and empirical assessment of stomatal optimization modeling. New 1261 1262 Phytologist, 227(2), 311–325. https://doi.org/10.1111/nph.16572 Williams, M., Rastetter, E. B., Fernandes, D. N., Goulden, M. L., Wofsy, S. C., Shaver, G. R., 1263 Melillo, J. M., Munger, J. W., Fan, S. M., & Nadelhoffer, K. J. (1996). Modelling the 1264 1265 soil-plant-atmosphere continuum in a *Quercus-Acer* stand at Harvard Forest: The regulation of stomatal conductance by light, nitrogen and soil/plant hydraulic properties. 1266 1267 Plant Cell, and Environment., 19(8), 911–927. https://doi.org/10.1111/j.1365-1268 3040.1996.tb00456.x Wohlfahrt, G., Hammerle, A., & Hörtnagl, L. (2002-2012). FLUXNET2015 AT-Neu Neustift 1269 [Dataset]. FLUXNET. https://doi.org/10.18140/FLX/1440121 1270

Wolf, A., Anderegg, W. R. L., & Pacala, S. W. (2016). Optimal stomatal behavior with 1271 competition for water and risk of hydraulic impairment. Proceedings of the National 1272 1273 Academy of Sciences, 113(46), E7222–E7230. https://doi.org/10.1073/pnas.1615144113 Woodgate, W., van Gorsel, E., Leuning, R., Kitchen, M., Hughes, D., & Zegelin, S. (2001-1274 2014). FLUXNET2015 AU-Tum Tumbarumba [Dataset]. FLUXNET. 1275 1276 https://doi.org/10.18140/FLX/1440126 Yamori, W., Hikosaka, K., & Way, D. A. (2014). Temperature response of photosynthesis in C<sub>3</sub>, 1277 C<sub>4</sub>, and CAM plants: Temperature acclimation and temperature adaptation. 1278 Photosynthesis Research, 119(1), 101–117. https://doi.org/10.1007/s11120-013-9874-6 1279 Yi, K., Maxwell, J. T., Wenzel, M. K., Roman, D. T., Sauer, P. E., Phillips, R. P., & Novick, K. 1280 A. (2019). Linking variation in intrinsic water-use efficiency to isohydricity: A 1281 comparison at multiple spatiotemporal scales. New Phytologist, 221(1), 195–208. 1282 https://doi.org/10.1111/nph.15384 1283 Yi, K., Smith, J. W., Jablonski, A. D., Tatham, E. A., Scanlon, T. M., Lerdau, M. T., Novick, K. 1284 A., & Yang, X. (2020). High heterogeneity in canopy temperature among co-occurring 1285 tree species in a temperate forest. Journal of Geophysical Research: Biogeosciences, 1286 1287 125(12), e2020JG005892. https://doi.org/10.1029/2020JG005892 Zhang, Q., Ficklin, D. L., Manzoni, S., Wang, L., Way, D., Phillips, R. P., & Novick, K. A. 1288 1289 (2019). Response of ecosystem intrinsic water use efficiency and gross primary 1290 productivity to rising vapor pressure deficit. Environmental Research Letters, 14(7), 074023. https://doi.org/10.1088/1748-9326/ab2603 1291 Zhou, S. X., Duursma, R. A., Medlyn, B. E., Kelly, J. W. G., & Prentice, I. C. (2013). How 1292 1293 should we model plant responses to drought? An analysis of stomatal and non-stomatal

1294	responses to water stress. Agricultural and Forest Meteorology, 182–183, 204–214.
1295	https://doi.org/10.1016/j.agrformet.2013.05.009
1296	Zhou, S. X., Medlyn, B., Sabate, S., Sperlich, D., & Prentice, I. C. (2014). Short-term water
1297	stress impacts on stomatal, mesophyll and biochemical limitations to photosynthesis
1298	differ consistently among tree species from contrasting climates. Tree Physiology,
1299	34(10), 1035–1046. https://doi.org/10.1093/treephys/tpu072